

Variable-Wise Diagonal Preconditioning for Primal-Dual Splitting: Design and Applications

Kazuki Naganuma, *Student Member, IEEE*, Shunsuke Ono, *Member, IEEE*,

Abstract—This paper proposes a method for designing diagonal preconditioners for a preconditioned primal-dual splitting method (P-PDS), an efficient algorithm that solves nonsmooth convex optimization problems. To speed up the convergence of P-PDS, a design method has been proposed to automatically determine appropriate preconditioners from the problem structure. However, the existing method has two limitations. One is that it directly accesses all elements of matrices representing linear operators involved in a given problem, which is inconvenient for handling linear operators implemented as procedures rather than matrices. The other is that it takes an element-wise preconditioning approach, which turns certain types of proximity operators into analytically intractable forms. To overcome these limitations, we establish an Operator norm-based design method of Variable-wise Diagonal Preconditioning (OVDP). First, OVDP constructs diagonal preconditioners using only (upper bounds) of the operator norms of linear operators, thus eliminating the need for their explicit matrix representations. Furthermore, since OVDP takes a variable-wise preconditioning approach, it keeps any proximity operator analytically computable. We also prove that our preconditioners satisfy the convergence condition of P-PDS. Finally, we demonstrate the effectiveness and usefulness of OVDP through applications to mixed noise removal of hyperspectral images, hyperspectral unmixing, and graph signal recovery.

Index Terms—Primal-dual splitting method (PDS), diagonal preconditioning, convex optimization, signal estimation

I. INTRODUCTION

Many signal estimation and processing problems, such as denoising, interpolation, decomposition, and reconstruction, have been resolved by casting them as convex optimization problems [1], [2] of the form:

$$\begin{aligned} \min_{\mathbf{x}_1, \dots, \mathbf{x}_N, \mathbf{y}_1, \dots, \mathbf{y}_M} \quad & \sum_{i=1}^N f_i(\mathbf{x}_i) + \sum_{j=1}^M g_j(\mathbf{y}_j) \\ \text{s.t. } \quad & \mathbf{y}_1 = \sum_{i=1}^N \mathcal{L}_{1,i}(\mathbf{x}_i), \dots, \mathbf{y}_M = \sum_{i=1}^N \mathcal{L}_{M,i}(\mathbf{x}_i), \end{aligned} \quad (1)$$

where $f_i : \mathbb{R}^{n_i} \rightarrow (-\infty, +\infty]$ and $g_j : \mathbb{R}^{m_j} \rightarrow (-\infty, +\infty]$ are proximable¹ proper lower-semicontinuous convex functions, and $\mathcal{L}_{j,i} : \mathbb{R}^{n_i} \rightarrow \mathbb{R}^{m_j}$ are bounded linear operators ($\forall i = 1, \dots, N$ and $\forall j = 1, \dots, M$). The variables

Manuscript received XXX, XXX; revised XXX XXX, XXX.

K. Naganuma is with the Department of Computer Science, Tokyo Institute of Technology, Yokohama, 226-8503, Japan (e-mail: naganuma.k.aa@m.titech.ac.jp).

S. Ono is with the Department of Computer Science, Tokyo Institute of Technology, Yokohama, 226-8503, Japan (e-mail: ono@c.titech.ac.jp).

This work was supported Grant-in-Aid for JSPS Fellows under Grant 23KJ0912, in part by JST PRESTO under Grant JPMJPR21C4 and JST AdCORP under Grant JPMJKB2307, and in part by JSPS KAKENHI under Grant 22H03610, 22H00512, and 23H01415.

$\mathbf{x}_1, \dots, \mathbf{x}_N$ represent estimated signals or components, and $\mathbf{y}_1, \dots, \mathbf{y}_M$ are auxiliary variables for splitting.

As a method for solving Prob. (1), a primal-dual splitting method (PDS) [3] has attracted attention [4]–[12] due to its simple implementation without operator inversions.² To improve the convergence speed of PDS, a preconditioned PDS (P-PDS) has been studied [15]–[18]. P-PDS is a generalization of the standard PDS, where scalar-valued stepsizes are replaced by (positive definite) matrix-valued preconditioners. The theoretical convergence of P-PDS is established in a primal-dual space equipped with a skewed metric, which is determined by the linear operators involved in the optimization problem and the preconditioners used (see [13], [15], [19] for details). Preconditioning can be viewed as the selection of an appropriate metric for optimization algorithms and is a crucial long-standing issue not only in P-PDS but also in various proximal algorithms [20], [21].

The appropriate preconditioners that accelerate the convergence of P-PDS vary greatly depending on the structure of the target optimization problem (see Section IV for detailed examples). To automatically determine such preconditioners, the authors in [15] have proposed a diagonal-preconditioner design method. The elements of the diagonal preconditioners consist of the row/column absolute sum of the elements of the explicit matrices representing the linear operators $\mathcal{L}_{j,i}$ in (1), and thus the resulting diagonal elements of the preconditioners can be different for each element in one variable.

Although this design method determines reasonable diagonal preconditioners, there exist two limitations that are considerable in real applications. First, the method is difficult to apply in the case where (some of) the linear operators $\mathcal{L}_{j,i}$ in Prob. (1) are not implemented as explicit matrices because it requires access to the entire elements of the matrices to construct the preconditioners. We often encounter such situations, especially in imaging applications, where the linear operators are implemented not as explicit matrices but as procedures that compute forward and adjoint operations in an efficient manner, e.g., difference operators [22], [23] and frame transforms [24]–[26]. Second, some proximable functions f_i and g_j are not completely separable for each element of the input variables \mathbf{x}_i and \mathbf{y}_j , e.g., mixed norms and the indicator functions of norm balls [27]. For such functions, the element-wise preconditioning might make the functions non-proximable.

¹If an efficient computation of the proximity operator (see. Eq. (3)) of f is available, we call f proximable.

²This algorithm has been generalized by Condat [13] and Vu [14], where smooth convex functions are optimized by using their Lipschitzian gradients.

To address the above issues, this paper proposes an Operator-norm-based design method of Variable-wise Diagonal Preconditioning (OVDP). Specifically, we introduce a new general form of P-PDS preconditioners, and then propose specific preconditioners based on this general form. We also prove that the sequence generated by P-PDS with OVDP converges to an optimal solution of Prob. (1).

Our method has two features preferred in many real-world applications. First, our preconditioners can be computed from (upper bounds of) the operator norms of the linear operators $\mathcal{L}_{j,i}$, meaning that our method does not need their explicit matrix representations. This is because (upper bounds of) the operator norms are often known or can be estimated without matrix implementation for typical linear operators used in signal processing, including the ones mentioned above. Second, the elements of the diagonal preconditioners obtained by our method take the same value for all the elements of each variable, i.e., variable-wise preconditioning. This maintains the proximability of the functions f_i and g_j in Prob. (1).

Comprehensive experiments are conducted by applying our method to three signal estimation problems: mixed noise removal of hyperspectral images, hyperspectral unmixing, and graph signal recovery. By discussing the convergence in these three optimization problems, which have very different structures, we demonstrate the effectiveness and usefulness of our method.

This paper is organized as follows. Section II gives preliminaries on mathematical tools, the description of P-PDS, and reviews of existing preconditioner design methods. In Section III, we present OVDP and prove the convergence theorem of P-PDS with OVDP. Their applications to mixed noise removal hyperspectral images, hyperspectral unmixing, and graph signal recovery are given in Section IV. Finally, we conclude the paper in Section V.

The preliminary version of this work, without the generalization of our method, applications to various signal estimation tasks, or deeper discussion, has appeared in conference proceedings [28].

II. PRELIMINARIES

A. Notations

In this paper, vectors and matrices are denoted by lowercase and uppercase bold letters, for example, \mathbf{x} and \mathbf{X} , respectively. For a vector $\mathbf{x} = [x_1, \dots, x_N]^T \in \mathbb{R}^N$, each scalar value x_i ($1 \leq i \leq N$) is called the i th element of \mathbf{x} . Similarly, for a matrix $\mathbf{X} = [x_{j,i}]_{1 \leq j \leq M, 1 \leq i \leq N}$, each scalar value $x_{j,i}$ ($1 \leq j \leq M, 1 \leq i \leq N$) is called the (j, i) th element of \mathbf{X} . We denote a matrix $\mathbf{X} \in \mathbb{R}^{\tilde{m} \times \tilde{n}}$ ($\tilde{m} = \sum_{j=1}^M m_j, \tilde{n} = \sum_{i=1}^N n_i$) consisting of block matrices $\mathbf{X}_{j,i} \in \mathbb{R}^{m_j \times n_i}$ ($j = 1, \dots, M$ and $i = 1, \dots, N$) by $\mathbf{X} = [\mathbf{X}_{j,i}]_{1 \leq j \leq M, 1 \leq i \leq N}$. Let $\mathcal{L} : \mathbb{R}^N \rightarrow \mathbb{R}^M$ be a linear operator. We denote the adjoint operator of \mathcal{L} as \mathcal{L}^* , which satisfies $\langle \mathcal{L}(\mathbf{x}), \mathbf{y} \rangle = \langle \mathbf{x}, \mathcal{L}^*(\mathbf{y}) \rangle$ for any $\mathbf{x} \in \mathbb{R}^N$ and $\mathbf{y} \in \mathbb{R}^M$.

B. Mathematical Tools

Let $f : \mathbb{R}^N \rightarrow (-\infty, \infty]$ be a proximable proper lower-semicontinuous convex function and $\mathbf{G} \in \mathbb{R}^{N \times N}$ be a sym-

metric and positive definite matrix. The proximity operator of f relative to the metric induced by \mathbf{G} is defined as

$$\text{prox}_{\mathbf{G},f}(\mathbf{x}) := \underset{\mathbf{y}}{\text{argmin}} \frac{1}{2} \langle \mathbf{x} - \mathbf{y}, \mathbf{G}(\mathbf{x} - \mathbf{y}) \rangle + f(\mathbf{y}), \quad (2)$$

where $\langle \cdot, \cdot \rangle$ is the Euclidean inner product. If \mathbf{G} is a positive scalar matrix, i.e., $\mathbf{G} = \alpha \mathbf{I}$ ($\alpha > 0$), the proximity operator is identical to the standard proximity operator:

$$\text{prox}_{\mathbf{G},f}(\mathbf{x}) = \underset{\mathbf{y}}{\text{argmin}} \frac{1}{2} \|\mathbf{x} - \mathbf{y}\|_2^2 + \frac{1}{\alpha} f(\mathbf{y}). \quad (3)$$

In this paper, the proximity operator relative to the metric induced by a positive matrix that is not scalar matrix is called the *skewed proximity operator*. We would like to note that the standard proximity operators of some popular convex functions, such as the mixed $\ell_{1,2}$ -norm and the indicator functions of norm balls, have analytic solutions but their computations are not completely separable element by element. In such cases, even if \mathbf{G} is diagonal (with different elements), the computation of the skewed proximity operator becomes difficult.

The *Fenchel–Rockafellar conjugate function* of f is defined as

$$f^*(\mathbf{x}) := \max_{\mathbf{y}} \langle \mathbf{x}, \mathbf{y} \rangle - f(\mathbf{y}). \quad (4)$$

Thanks to the generalization of Moreau’s Identity [29, Theorem 3.1 (ii)], the skewed proximity operator of f^* is calculated as

$$\text{prox}_{\mathbf{G},f^*}(\mathbf{x}) = \mathbf{x} - \mathbf{G}^{-1} \text{prox}_{\mathbf{G}^{-1},f}(\mathbf{G}\mathbf{x}). \quad (5)$$

For a given nonempty closed convex set $C \subset \mathbb{R}^N$, the indicator function of C is defined by

$$\iota_C(\mathcal{X}) := \begin{cases} 0, & \text{if } \mathcal{X} \in C; \\ \infty, & \text{otherwise.} \end{cases} \quad (6)$$

The proximity operator of the indicator function ι_C is equivalent to the convex projection onto C . The following convex sets are useful in signal processing.

- The \mathbf{c} -centered ℓ_p -ball with the radius $\alpha > 0$ defined by

$$B_{p,\alpha}^{\mathbf{c}} := \{\mathbf{x} \in \mathbb{R}^N \mid \|\mathbf{x} - \mathbf{c}\|_p \leq \alpha\}. \quad (7)$$

- The nonnegative orthant $\mathbb{R}_+^N := [0, +\infty)^N$.

For a linear operator \mathcal{L} , the operator norm $\|\mathcal{L}\|_{\text{op}}$ is defined by

$$\|\mathcal{L}\|_{\text{op}} := \sup_{\mathbf{x} \neq \mathbf{0}} \frac{\|\mathcal{L}(\mathbf{x})\|_2}{\|\mathbf{x}\|_2}. \quad (8)$$

For a matrix \mathbf{A} , its operator norm satisfies

$$\|\mathbf{A}\|_{\text{op}} := \sup_{\mathbf{x} \neq \mathbf{0}} \frac{\|\mathbf{A}\mathbf{x}\|_2}{\|\mathbf{x}\|_2} = \sigma_1(\mathbf{A}), \quad (9)$$

where $\sigma_1(\mathbf{A})$ is the maximum singular value of \mathbf{A} . Let $\mathcal{L}_1 \circ \mathcal{L}_2$ be the composition of linear operators \mathcal{L}_1 and \mathcal{L}_2 . The operator norm of $\mathcal{L}_1 \circ \mathcal{L}_2$ satisfies that

$$\|\mathcal{L}_1 \circ \mathcal{L}_2\|_{\text{op}} \leq \|\mathcal{L}_1\|_{\text{op}} \|\mathcal{L}_2\|_{\text{op}}. \quad (10)$$

This property is called *the submultiplicity*.

C. Preconditioned PDS (P-PDS)

For Prob. (1), let $\mathbf{x} = [\mathbf{x}_1^\top, \dots, \mathbf{x}_N^\top]^\top \in \mathbb{R}^{\tilde{n}}$ ($\tilde{n} = \sum_{i=1}^N n_i$), $\mathbf{y} = [\mathbf{y}_1^\top, \dots, \mathbf{y}_M^\top]^\top \in \mathbb{R}^{\tilde{m}}$ ($\tilde{m} = \sum_{j=1}^M m_j$), $f(\mathbf{x}) = \sum_{i=1}^N f_i(\mathbf{x}_i)$, $g(\mathbf{y}) = \sum_{j=1}^M g_j(\mathbf{y}_j)$, and

$$\mathfrak{L} := \begin{bmatrix} \mathfrak{L}_{1,1} & \mathfrak{L}_{1,2} & \cdots & \mathfrak{L}_{1,N} \\ \mathfrak{L}_{2,1} & \mathfrak{L}_{2,2} & \cdots & \mathfrak{L}_{2,N} \\ \vdots & \vdots & \ddots & \vdots \\ \mathfrak{L}_{M,1} & \mathfrak{L}_{M,2} & \cdots & \mathfrak{L}_{M,N} \end{bmatrix}. \quad (11)$$

P-PDS [15] computes an optimal solution of Prob. (1) by the following iterative procedures:

$$\begin{cases} \mathbf{x}^{(t+1)} \leftarrow \text{prox}_{\Gamma_1^{-1}, f}(\mathbf{x}^{(t)} - \Gamma_1 \mathfrak{L}^*(\mathbf{y}^{(t)})), \\ \mathbf{y}^{(t+1)} \leftarrow \text{prox}_{\Gamma_2^{-1}, g^*}(\mathbf{y}^{(t)} + \Gamma_2 \mathfrak{L}(2\mathbf{x}^{(t+1)} - \mathbf{x}^{(t)})), \end{cases} \quad (12)$$

where $\Gamma_1 \in \mathbb{R}^{\tilde{n} \times \tilde{n}}$ and $\Gamma_2 \in \mathbb{R}^{\tilde{m} \times \tilde{m}}$ are symmetric and positive definite matrices called *preconditioners*.

If Γ_1 and Γ_2 are block-diagonal matrices, that is, $\Gamma_1 = \text{diag}(\Gamma_{1,1}, \dots, \Gamma_{1,N})$ and $\Gamma_2 = \text{diag}(\Gamma_{2,1}, \dots, \Gamma_{2,M})$ for matrices $\Gamma_{1,1}, \dots, \Gamma_{1,N}, \Gamma_{2,1}, \dots, \Gamma_{2,M}$ corresponding to $\mathbf{x}_1, \dots, \mathbf{x}_N, \mathbf{y}_1, \dots, \mathbf{y}_M$, the procedures in (12) can be rewritten as the following equivalent form:

$$\begin{cases} \mathbf{x}_1^{(t+1)} \leftarrow \text{prox}_{\Gamma_{1,1}^{-1}, f_1}(\mathbf{x}_1^{(t)} - \Gamma_{1,1} \sum_{j=1}^M \mathfrak{L}_{j,1}^*(\mathbf{y}_j^{(t)})), \\ \vdots \\ \mathbf{x}_N^{(t+1)} \leftarrow \text{prox}_{\Gamma_{1,N}^{-1}, f_N}(\mathbf{x}_N^{(t)} - \Gamma_{1,N} \sum_{j=1}^M \mathfrak{L}_{j,N}^*(\mathbf{y}_j^{(t)})), \\ \mathbf{y}_1^{(t+1)} \leftarrow \text{prox}_{\Gamma_{2,1}^{-1}, g_1^*}(\mathbf{y}_1^{(t)} + \Gamma_{2,1} \sum_{i=1}^N \mathfrak{L}_{1,i}(2\mathbf{x}_i^{(t+1)} - \mathbf{x}_i^{(t)})), \\ \vdots \\ \mathbf{y}_M^{(t+1)} \leftarrow \text{prox}_{\Gamma_{2,M}^{-1}, g_M^*}(\mathbf{y}_M^{(t)} + \Gamma_{2,M} \sum_{i=1}^N \mathfrak{L}_{j,i}(2\mathbf{x}_i^{(t+1)} - \mathbf{x}_i^{(t)})). \end{cases} \quad (13)$$

Compared with (12), the procedures in (13) can easily be calculated because it avoids the computations of the skewed proximity operators and linear operators over the entire variables.

Here, we introduce the convergence theorem of P-PDS.

Theorem II.1. [15, Theorem 1] *Let Γ_1 and Γ_2 be symmetric and positive definite matrices satisfying*

$$\left\| \Gamma_2^{\frac{1}{2}} \circ \mathfrak{L} \circ \Gamma_1^{\frac{1}{2}} \right\|_{\text{op}}^2 < 1. \quad (14)$$

Then, the sequence $(\mathbf{x}_1^{(t)}, \dots, \mathbf{x}_N^{(t)}, \mathbf{y}_1^{(t)}, \dots, \mathbf{y}_M^{(t)})$ generated by (12) converges to an optimal solution $(\mathbf{x}_1^, \dots, \mathbf{x}_N^*, \mathbf{y}_1^*, \dots, \mathbf{y}_M^*)$ of Prob. (1).*

D. Existing Preconditioner Design Methods

1) *Scalar Preconditioning (SP)*: The standard PDS [3] can be recovered by setting the scalar preconditioners as

$$\Gamma_1 = \gamma_1 \mathbf{I}, \Gamma_2 = \gamma_2 \mathbf{I}. \quad (15)$$

The parameters γ_1 and γ_2 are positive scalars that satisfy (14), that is,

$$\gamma_1 \gamma_2 \|\mathfrak{L}\|_{\text{op}}^2 < 1. \quad (16)$$

In real situations, the parameter γ_2 is often set as

$$\gamma_2 = \frac{1}{\mu_{SP}^2 \gamma_1}, \quad (17)$$

where μ_{SP} is an upper bound of $\|\mathfrak{L}\|_{\text{op}}$. Since $\|\mathfrak{L}\|_{\text{op}} < \mu_{SP}$, the parameters γ_1 and γ_2 in (17) satisfy the inequality in (16). We note that the parameter γ_1 needs to be manually adjusted for accelerating the convergence of P-PDS.

2) *Row/Column Absolute Sum-Based Element-Wise Preconditioning (ASP)*: Let $\mathbf{L}_{j,i}$ be the representation matrix of $\mathfrak{L}_{j,i}$. The authors of [15] present a design method of constructing the preconditioners $\Gamma_1 = \text{diag}(\Gamma_{1,1}, \dots, \Gamma_{1,N})$ and $\Gamma_2 = \text{diag}(\Gamma_{2,1}, \dots, \Gamma_{2,M})$ as follows:

$$\begin{aligned} \Gamma_{1,i} &= \text{diag} \left(\frac{1}{\sigma_{i,1}}, \dots, \frac{1}{\sigma_{i,n_i}} \right), \quad (\forall i = 1, \dots, N), \\ \Gamma_{2,j} &= \text{diag} \left(\frac{1}{\tau_{j,1}}, \dots, \frac{1}{\tau_{j,m_j}} \right), \quad (\forall j = 1, \dots, M), \end{aligned} \quad (18)$$

where

$$\begin{aligned} \sigma_{i,l} &= \sum_{j=1}^M \sum_{k=1}^{m_j} |[\mathbf{L}_{j,i}]_{k,l}|, \quad (\forall l = 1, \dots, n_i), \\ \tau_{j,l} &= \sum_{i=1}^N \sum_{k=1}^{n_i} |[\mathbf{L}_{j,i}]_{1,k}|, \quad (\forall l = 1, \dots, m_j). \end{aligned} \quad (19)$$

Each $\Gamma_{1,i}$ (or $\Gamma_{2,j}$) is a diagonal matrix consisting of the row/column absolute sums of the elements of $\mathbf{L}_{j,i}$ (see [15, Lemma 2]). This means that the diagonal elements of one $\Gamma_{1,i}$ (and $\Gamma_{2,j}$) may take different values, i.e., the diagonal elements of the preconditioners will be different for each element for one variable in (1).

3) *Positive-Definite Preconditioning (PDP)*: The authors in [18] proposed to determine the preconditioners as

$$\Gamma_1 = \tau \mathbf{I}, \Gamma_2 = \frac{1}{\tau} (\mathbf{L} \mathbf{L}^\top + \theta \mathbf{I})^{-1}, \quad (20)$$

where \mathbf{L} is the representation matrix of \mathfrak{L} and $\tau > 0$ is a parameter. Since the preconditioners in (20) are not block-diagonal matrices in general, the P-PDS with them results in the procedures given in (12).

If the number of dual variables is two ($M = 2$), the preconditioners are set as

$$\Gamma_1 = \frac{\tau}{2} \mathbf{I}, \Gamma_2 = \begin{bmatrix} \Gamma_{2,1} & \mathbf{O} \\ \mathbf{O} & \Gamma_{2,2} \end{bmatrix}, \quad (21)$$

where

$$\Gamma_{2,j} = \frac{1}{\tau} \left(\sum_{i=1}^N \mathbf{L}_{j,i} \mathbf{L}_{j,i}^\top + \theta \mathbf{I} \right)^{-1}, \quad (\forall j = 1, 2). \quad (22)$$

Since Γ_1 and Γ_2 in (21) are block-diagonal matrices, P-PDS with them can solve the Prob. (1) by the procedures given in (13).

We note that the parameters τ and θ affect the convergence speed of P-PDS. Therefore, the parameters τ and θ need to be manually adjusted.

III. PROPOSED OPERATOR NORM-BASED VARIABLE-WISE DIAGONAL PRECONDITIONING (OVDP)

This section is devoted to the establishment of a novel diagonal preconditioning method, OVDP, for P-PDS. First, we introduce a general form of our preconditioners as follows: for all $i = 1, \dots, N$ and $\forall j = 1, \dots, M$

$$\begin{aligned}\Gamma_{1,i} &= \Gamma_{1,i} \mathbf{I} = \frac{1}{\sum_{j=1}^M \mu_{j,i}^{2-\beta}} \mathbf{I}, \\ \Gamma_{2,j} &= \Gamma_{2,j} \mathbf{I} = \frac{1}{\sum_{i=1}^N \mu_{j,i}^\beta} \mathbf{I}, \quad (\beta \in [0, 2])\end{aligned}\quad (23)$$

where each $\mu_{j,i}$ is an upper bound of the operator norm of each $\mathfrak{L}_{j,i}$, i.e.,

$$\mu_{j,i} \in [\|\mathfrak{L}_{j,i}\|_{\text{op}}, \infty). \quad (24)$$

By changing the choice of β , OVDP gives three design ways.

- If we choose $\beta = 0$, the preconditioners by OVDP (OVDP1) become

$$\Gamma_{1,i} = \frac{1}{\sum_{j=1}^M \mu_{j,i}^2} \mathbf{I}, \quad \Gamma_{2,j} = \frac{1}{N} \mathbf{I}. \quad (25)$$

- If we choose $\beta = 1$, the preconditioners by OVDP (OVDP2) become

$$\Gamma_{1,i} = \frac{1}{\sum_{j=1}^M \mu_{j,i}} \mathbf{I}, \quad \Gamma_{2,j} = \frac{1}{\sum_{i=1}^N \mu_{j,i}} \mathbf{I}. \quad (26)$$

- If we choose $\beta = 2$, the preconditioners by OVDP (OVDP3) become

$$\Gamma_{1,i} = \frac{1}{M} \mathbf{I}, \quad \Gamma_{2,j} = \frac{1}{\sum_{i=1}^N \mu_{j,i}^2} \mathbf{I}, \quad (27)$$

Remark III.1. Our method has the following two features.

- Our preconditioners can be calculated by only using (upper bounds of) the operator norms of the linear operators $\mathfrak{L}_{j,i}$. This implies that OVDP does not require direct access to the elements of the explicit matrices representing $\mathfrak{L}_{j,i}$ as long as some $\mu_{i,j}$ are available.
- In addition, the diagonal elements of one $\Gamma_{1,i}$ take the same value ($\Gamma_{2,j}$ as well), i.e., our method is a variable-wise preconditioning method, which maintains the proximability of the functions in Prob. (1).

Before showing the convergence theorem of P-PDS with OVDP defined in (23), we give the following lemma on matrix decomposition.

Lemma III.1. An arbitrary matrix $\mathbf{A} \in \mathbb{R}^{m \times n}$ can be decomposed into matrices \mathbf{B} and \mathbf{C} (i.e., $\mathbf{A} = \mathbf{BC}$) that satisfy for any $\beta \in [0, 1]$

$$\begin{aligned}\|\mathbf{B}\|_{\text{op}} &= \|\mathbf{A}\|_{\text{op}}^{1-\beta} (= \sigma_1(\mathbf{A})^{1-\beta}), \\ \|\mathbf{C}\|_{\text{op}} &= \|\mathbf{A}\|_{\text{op}}^\beta (= \sigma_1(\mathbf{A})^\beta).\end{aligned}\quad (28)$$

The proof is in Appendix.

Then, the following theorem guarantees the convergence of P-PDS with OVDP.

Algorithm 1 P-PDS with OVDP for solving (1)

Input: $\mathbf{x}_1^{(0)}, \dots, \mathbf{x}_N^{(0)}, \mathbf{y}_1^{(0)}, \dots, \mathbf{y}_M^{(0)}$
Output: $\mathbf{x}_1^{(t)}, \dots, \mathbf{x}_N^{(t)}, \mathbf{y}_1^{(t)}, \dots, \mathbf{y}_M^{(t)}$

- 1: Initialize $t = 0$;
- 2: Set $\Gamma_{1,1}, \dots, \Gamma_{1,N}, \Gamma_{2,1}, \dots, \Gamma_{2,M}$ as in (23);
- 3: **while** A stopping criterion is not satisfied **do**
- 4: **for** $i = 1, \dots, N$ **do**
- 5: $\mathbf{x}'_i \leftarrow \sum_{j=1}^M \mathfrak{L}_{j,i}^*(\mathbf{y}_j^{(t)})$;
- 6: $\mathbf{x}_i^{(t+1)} \leftarrow \text{prox}_{\Gamma_{1,i}^{-1}, f_i}(\mathbf{x}'_i - \Gamma_{1,i} \mathbf{x}'_i)$;
- 7: **end for**
- 8: **for** $j = 1, \dots, M$ **do**
- 9: $\mathbf{y}'_j \leftarrow \sum_{i=1}^N \mathfrak{L}_{j,i}(2\mathbf{x}_i^{(t+1)} - \mathbf{x}_i^{(t)})$;
- 10: $\mathbf{y}_j^{(t+1)} \leftarrow \text{prox}_{\Gamma_{2,j}^{-1}, g_j}(\mathbf{y}'_j + \Gamma_{2,j} \mathbf{y}'_j)$;
- 11: **end for**
- 12: $t \leftarrow t + 1$;
- 13: **end while**

Theorem III.2. If the preconditioners are set as (23), then the following inequality holds:

$$\left\| \Gamma_2^{\frac{1}{2}} \circ \mathfrak{L} \circ \Gamma_1^{\frac{1}{2}} \right\|_{\text{op}}^2 \leq 1. \quad (29)$$

Proof. Since Γ_1 and Γ_2 are positive-definite and diagonal, their powers of one-half are

$$\begin{aligned}\Gamma_1^{\frac{1}{2}} &= \text{diag} \left(\Gamma_{1,1}^{\frac{1}{2}}, \dots, \Gamma_{1,N}^{\frac{1}{2}} \right), \\ \Gamma_2^{\frac{1}{2}} &= \text{diag} \left(\Gamma_{2,1}^{\frac{1}{2}}, \dots, \Gamma_{2,M}^{\frac{1}{2}} \right).\end{aligned}\quad (30)$$

By matrix multiplication and Eq. (30), we have

$$\Gamma_2^{\frac{1}{2}} \circ \mathfrak{L} \circ \Gamma_1^{\frac{1}{2}} = \left[\Gamma_{2,j}^{\frac{1}{2}} \circ \mathfrak{L}_{j,i} \circ \Gamma_{1,i}^{\frac{1}{2}} \right]_{1 \leq i \leq N, 1 \leq j \leq M}. \quad (31)$$

From the inequality of the operator norm of a block matrix [30] and Eq. (23), we obtain

$$\left\| \Gamma_2^{\frac{1}{2}} \circ \mathfrak{L} \circ \Gamma_1^{\frac{1}{2}} \right\|_{\text{op}}^2 \leq \sum_{i=1}^N \sum_{j=1}^M \left\| \Gamma_{2,j}^{\frac{1}{2}} \circ \mathfrak{L}_{j,i} \circ \Gamma_{1,i}^{\frac{1}{2}} \right\|_{\text{op}}^2. \quad (32)$$

Since $\mathfrak{L}_{j,i}$ ($i = 1, \dots, N, j = 1, \dots, M$) are bounded linear operators, i.e., they can be represented by matrices, from Lemma III.1, there exist bounded linear operators $\mathfrak{L}_{j,i}^{\frac{\beta}{2}}$ and $\mathfrak{L}_{j,i}^{1-\frac{\beta}{2}}$ that satisfy for any $\beta \in [0, 2]$,

$$\begin{aligned}\mathfrak{L}_{j,i} &= \mathfrak{L}_{j,i}^{1-\frac{\beta}{2}} \circ \mathfrak{L}_{j,i}^{\frac{\beta}{2}}, \\ \|\mathfrak{L}_{j,i}^{1-\frac{\beta}{2}}\|_{\text{op}} &= \|\mathfrak{L}_{j,i}\|_{\text{op}}^{1-\frac{\beta}{2}}, \\ \|\mathfrak{L}_{j,i}^{\frac{\beta}{2}}\|_{\text{op}} &= \|\mathfrak{L}_{j,i}\|_{\text{op}}^{\frac{\beta}{2}}.\end{aligned}\quad (33)$$

Thus, it follows from the submultiplicity in (10)

$$\begin{aligned}
 & \left\| \Gamma_{\frac{1}{2}} \circ \mathcal{L} \circ \Gamma_{\frac{1}{2}} \right\|_{\text{op}}^2 \\
 & \leq \sum_{i=1}^N \sum_{j=1}^M \left\| \Gamma_{\frac{1}{2},j} \circ \mathcal{L}_{j,i}^{1-\frac{\beta}{2}} \circ \mathcal{L}_{j,i}^{\frac{\beta}{2}} \circ \Gamma_{\frac{1}{2},i} \right\|_{\text{op}}^2 \\
 & \leq \sum_{i=1}^N \Gamma_{1,i} \sum_{j=1}^M \Gamma_{2,j} \|\mathcal{L}_{j,i}\|_{\text{op}}^{2-\beta} \|\mathcal{L}_{j,i}\|_{\text{op}}^{\beta}. \quad (34)
 \end{aligned}$$

By applying the Cauchy-Schwarz inequality and the inequality $\sum_{j=1}^M x_j^2 \leq (\sum_{j=1}^M x_j)^2$ for any positive real numbers x_1, \dots, x_M , we obtain

$$\begin{aligned}
 & \left\| \Gamma_{\frac{1}{2}} \circ \mathcal{L} \circ \Gamma_{\frac{1}{2}} \right\|_{\text{op}}^2 \\
 & \leq \sum_{i=1}^N \Gamma_{1,i} \left(\sum_{j=1}^M \sqrt{\Gamma_{2,j}} \|\mathcal{L}_{j,i}\|_{\text{op}}^{1-\frac{\beta}{2}} \|\mathcal{L}_{j,i}\|_{\text{op}}^{\frac{\beta}{2}} \right)^2 \\
 & \leq \sum_{i=1}^N \Gamma_{1,i} \left(\sum_{j=1}^M \|\mathcal{L}_{j,i}\|_{\text{op}}^{2-\beta} \right) \left(\sum_{j=1}^M \Gamma_{2,j} \|\mathcal{L}_{j,i}\|_{\text{op}}^{\beta} \right). \quad (35)
 \end{aligned}$$

Then, the definitions of $\Gamma_{1,i}$ and $\Gamma_{2,j}$ yield $\sum_{j=1}^M \|\mathcal{L}_{j,i}\|_{\text{op}}^{2-\beta} \leq \sum_{j=1}^M \mu_{j,i}^{2-\beta}$ and $\sum_{i=1}^N \|\mathcal{L}_{j,i}\|_{\text{op}}^{\beta} \leq \sum_{i=1}^N \mu_{j,i}^{\beta}$ for any $i = 1, \dots, N$ and $j = 1, \dots, M$. Hence, Eq. (35) can be transformed into

$$\begin{aligned}
 \left\| \Gamma_{\frac{1}{2}} \circ \mathcal{L} \circ \Gamma_{\frac{1}{2}} \right\|_{\text{op}}^2 & \leq \sum_{i=1}^N \sum_{j=1}^M \Gamma_{2,j} \|\mathcal{L}_{j,i}\|_{\text{op}}^{\beta} \\
 & = \sum_{j=1}^M \Gamma_{2,j} \sum_{i=1}^N \|\mathcal{L}_{j,i}\|_{\text{op}}^{\beta} \leq 1. \quad (36)
 \end{aligned}$$

□

Remark III.3. To guarantee the convergence of P-PDS, inequality (14) has to be strict, but inequality (29) is not. However, we do not observe any convergence issue of P-PDS with our preconditioners in the experiments (see Section IV). This is because, our method separates \mathcal{L} variable by variable and sums up upper bounds of the operator norms, resulting in setting preconditioners such that $\|\Gamma_{\frac{1}{2}} \circ \mathcal{L} \circ \Gamma_{\frac{1}{2}}\|_{\text{op}}^2 < 1$ in almost all real-world applications.

Theorem III.2 asserts that our preconditioners defined in (25), (26), and (27) satisfy the convergence condition of P-PDS in (14) of P-PDS. Therefore, P-PDS with OVDP generates sequences that converge to an optimal solution of Prob. (1).

Here, each $\mu_{j,i}$ is determined in the following manner.

- If the operator norm $\|\mathcal{L}_{j,i}\|_{\text{op}}$ is known, we set $\mu_{j,i}$ to $\|\mathcal{L}_{j,i}\|_{\text{op}}$.
- If $\|\mathcal{L}_{j,i}\|_{\text{op}}$ is unknown, we set $\mu_{j,i}$ to an upper bound of $\|\mathcal{L}_{j,i}\|_{\text{op}}$.
- If the linear operator is the composition of two linear operators \mathfrak{A} and \mathfrak{B} whose operator norms (or their upper bounds) are known ($\|\mathfrak{A}\|_{\text{op}} \leq \alpha_{\mathfrak{A}}$, $\|\mathfrak{B}\|_{\text{op}} \leq \alpha_{\mathfrak{B}}$), we set $\mu_{j,i}$ to $\alpha_{\mathfrak{A}}\alpha_{\mathfrak{B}}$, which is an upper bound of $\|\mathfrak{A} \circ \mathfrak{B}\|_{\text{op}}$ due to the submultiplicity in (10).

TABLE I
FEATURES OF EXISTING METHODS
AND OUR METHOD (HIGHLIGHTED IN BOLD).

| Methods | Parameters requiring manual adjustment | Maintaining proximabilities | Avoiding access to representation matrix |
|--------------|--|-----------------------------|--|
| SP [3] | γ_1 | ✓ | ✓ |
| ASP [15] | None. | × | × |
| PDP [18] | τ | × | ✓ |
| OVDP1 | None. | ✓ | ✓ |
| OVDP2 | None. | ✓ | ✓ |
| OVDP3 | None. | ✓ | ✓ |

TABLE II
STOPPING CRITERIA.

| Applications | Stopping criteria |
|-----------------------|-------------------|
| Mixed noise removal | RMSE < 0.005 |
| Unmixing | RMSE < 0.01 |
| Graph signal recovery | RMSE < 0.001 |

Finally, we show the detailed procedures of P-PDS with OVDP in Algorithm 1.

IV. EXPERIMENTS AND DISCUSSION

In this section, we apply our OVDP to three signal estimation problems: mixed noise removal of hyperspectral images, hyperspectral unmixing, and graph signal recovery. Through these applications, we illustrate the following effectiveness and usefulness of our method as follows:

- P-PDS with OVDP is fast on average to obtain an optimal solution of the target optimization problem.
- The preconditioners by OVDP can be easily calculated by using operator norms even if the target optimization problem involves the linear operators implemented not as explicit matrices.
- P-PDS with OVDP is efficiently computed by avoiding the computations of skewed proximity operators.

A. Experimental Setup

We compared OVDP with three existing preconditioner design methods (see Tab. I): the Scalar Preconditioning (SP) [3] in (15), the row/column Absolute Sum-based element-wise Preconditioning (ASP) [15] in (18), and the Positive-Definite Preconditioning (PDP) [18] in (20) and in (21). Note that the preconditioners by SP and PDP have parameters (γ_1, τ, θ) to be adjusted manually. For SP, we set γ_1 and γ_2 in (15) as $\gamma_1 = 1, 0.1, 0.01, 0.001$, and as in (17). The parameter τ in (20) and in (21) was set as $\tau = 1, 0.1, 0.01, 0.001$. The parameter θ in (20) and in (21) was set as $\theta = 0.01$, which is recommended in [18]. To calculate skewed proximity operators in the iterations of P-PDSs with ASP and PDP, we used the Fast Iterative Shrinkage-Thresholding Algorithm (FISTA) [31] initialized with a zero vector.

To check the convergence of P-PDS, we used the Root Mean Square Error (RMSE):

$$\text{RMSE}(\mathbf{x}_1^{(t)}, \dots, \mathbf{x}_N^{(t)}) := \sqrt{\frac{\sum_{i=1}^N \|\mathbf{x}_i^{(t)} - \mathbf{x}_i^*\|_2^2}{\sum_{i=1}^N n_i}}, \quad (37)$$

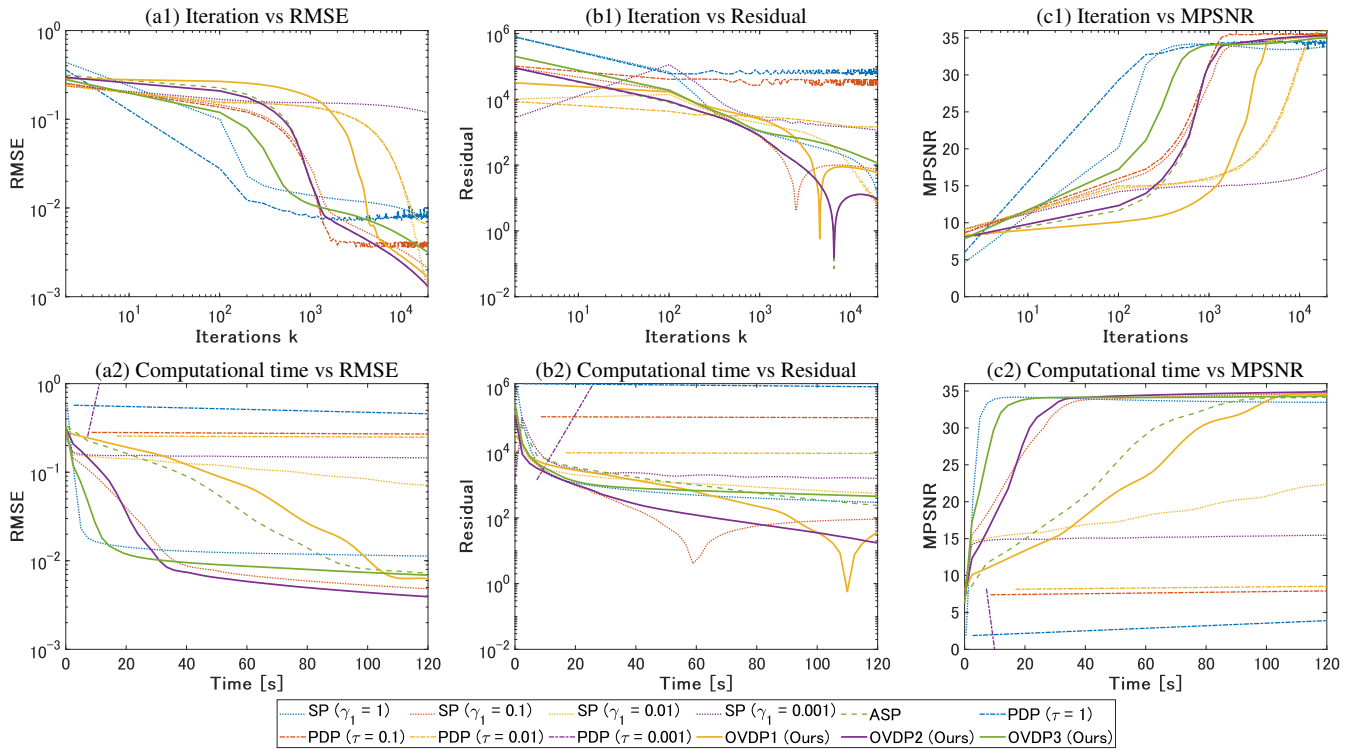


Fig. 1. Convergence profiles of the mixed noise removal experiments. (a): Iterations/computational time versus RMSE. (b): Iterations/computational time versus Residual. (c): Iterations/computational time versus MPSNR. Note that applying P-PDS with ASP (green dotted line) to Prob. (40) is not practical in terms of implementation (the linear operators \mathcal{D}_v , \mathcal{D}_h , and \mathcal{D}_b are not usually implemented as explicit matrices).

and the residual of the function values:

$$\begin{aligned} & \text{Residual}(\mathbf{x}_1^{(t)}, \dots, \mathbf{x}_N^{(t)}) \\ & := \left| \left(\sum_{i=1}^N f_i(\mathbf{x}_i^{(t)}) + \sum_{j=1}^M g_j \left(\sum_{i=1}^N \mathcal{L}_{j,i}(\mathbf{x}_i^{(t)}) \right) \right) \right. \\ & \quad \left. - \left(\sum_{i=1}^N f_i(\mathbf{x}_i^*) + \sum_{j=1}^M g_j \left(\sum_{i=1}^N \mathcal{L}_{j,i}(\mathbf{x}_i^*) \right) \right) \right|, \quad (38) \end{aligned}$$

where $\mathbf{x}_1^*, \dots, \mathbf{x}_N^*$ are oracle solutions. However, such oracle solutions are not available in the experiments, and therefore, we generated pseudo-oracle solutions by the following procedures. We calculated the results through 100,000 iterations of P-PDS with all the methods in advance, and then selected the best ones among them.

Tab. II shows the stopping criteria with RMSE as the threshold used in the experiments. Since convergence speeds are different depending on problems, reasonable criteria are also different. To determine reasonable criteria, we employed normalized error ($\|\mathbf{x}^{(t+1)} - \mathbf{x}^{(t)}\|_2 / \|\mathbf{x}^{(t)}\|_2$), which is often used as stopping criteria in real-world applications. Based on the normalized error, we set the stopping criteria as the RMSE values such that $\|\mathbf{x}^{(t+1)} - \mathbf{x}^{(t)}\|_2 / \|\mathbf{x}^{(t)}\|_2 < 10^{-5}$.

B. Application to Mixed Noise Removal of Hyperspectral Images

Hyperspectral (HS) images often suffer from various noises, such as random noise, outliers, missing values, and stripe noise, due to environmental and sensor issues [32]–[34]. These noises seriously degrade the performance of subsequent

processing, such as HS unmixing [35], classification [36], and anomaly detection [37]. Therefore, removing mixed noise from HS images is a crucial preprocessing. Popular mixed noise removal methods adopt the Spatio-Spectral Total Variation (SSTV) regularization [38]–[44], which models the spatial piecewise-smoothness and the spectral correlations of HS images.

1) *Problem Formulation:* Consider that an observed HS image (of size $N_1 \times N_2 \times N_3$) $\mathbf{v} \in \mathbb{R}^{N_1 N_2 N_3}$ is given by

$$\mathbf{v} = \bar{\mathbf{u}} + \bar{\mathbf{s}} + \bar{\mathbf{l}} + \mathbf{n}, \quad (39)$$

where $\bar{\mathbf{u}}$, $\bar{\mathbf{s}}$, $\bar{\mathbf{l}}$, and \mathbf{n} are the true HS image of interest, sparsely distributed noise (e.g. outliers and missing values), stripe noise, and random noise, respectively. Based on this observation model, the SSTV-regularized mixed noise removal problem is formulated as the following convex optimization problem:

$$\begin{aligned} & \min_{\mathbf{u}, \mathbf{s}, \mathbf{l}} \|\mathcal{D}_v(\mathcal{D}_b(\mathbf{u}))\|_1 + \|\mathcal{D}_h(\mathcal{D}_b(\mathbf{u}))\|_1 + \lambda \|\mathbf{l}\|_1 \\ & \text{s.t. } \mathcal{D}_v(\mathbf{l}) = \mathbf{0}, \mathbf{s} \in B_{1, \eta_s}^0, \mathbf{u} + \mathbf{s} + \mathbf{l} \in B_{2, \varepsilon}^y, \quad (40) \end{aligned}$$

where \mathcal{D}_v , \mathcal{D}_h , and \mathcal{D}_b are the vertical, horizontal, and spectral difference operators, respectively, with the Neumann boundary condition. To reduce computing resources, these difference operators are usually implemented not as matrices but as the following procedures:

$$[\mathcal{D}_v(\mathbf{x})]_{i,j,k} := \begin{cases} [\mathbf{x}]_{i,j,k} - [\mathbf{x}]_{i+1,j,k}, & \text{if } i < N_1; \\ 0, & \text{otherwise,} \end{cases} \quad (41)$$

$$[\mathcal{D}_h(\mathbf{x})]_{i,j,k} := \begin{cases} [\mathbf{x}]_{i,j,k} - [\mathbf{x}]_{i,j+1,k}, & \text{if } j < N_2; \\ 0, & \text{otherwise,} \end{cases} \quad (42)$$

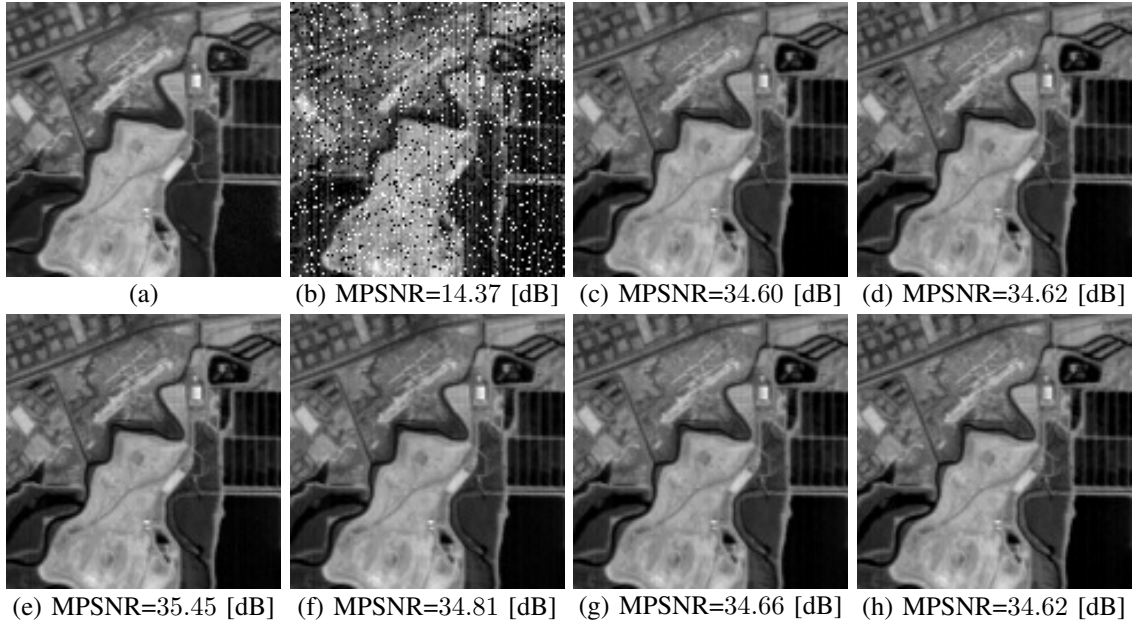


Fig. 2. Mixed noise removal results. (a): The ground truth HS image. (b): The observed HS image. (c): The HS image estimated by P-PDS with SP [3] ($\gamma_1 = 0.1$). (d): The HS image estimated by P-PDS with ASP [15]. (e): The HS image estimated by P-PDS with PDP [18] ($\tau = 0.1$). (f): The HS image estimated by P-PDS with OVDPI (Ours). (g): The HS image estimated by P-PDS with OVDP2 (Ours). (h): The HS image estimated by P-PDS with OVDP3 (Ours).

$$[\mathcal{D}_b(\mathbf{x})]_{i,j,k} := \begin{cases} [\mathbf{x}]_{i,j,k} - [\mathbf{x}]_{i,j,k+1}, & \text{if } k < N_3; \\ 0, & \text{otherwise,} \end{cases} \quad (43)$$

where $[\mathbf{x}]_{i_1, i_2, i_3}$ is the value of \mathbf{x} at a location (i_1, i_2, i_3) . Here, $\|\cdot\|_1$ is the ℓ_1 norm, and $B_{2,\varepsilon}^{\mathbf{y}}$ and $B_{1,\eta_s}^{\mathbf{0}}$ are the ℓ_2 and ℓ_1 norm balls, respectively given by

$$\begin{aligned} B_{2,\varepsilon}^{\mathbf{y}} &:= \{\mathbf{x} \in \mathbb{R}^{N_1 N_2 N_3} \mid \|\mathbf{v} - \mathbf{x}\|_2 \leq \varepsilon\}, \\ B_{1,\eta_s}^{\mathbf{0}} &:= \{\mathbf{x} \in \mathbb{R}^{N_1 N_2 N_3} \mid \|\mathbf{x}\|_1 \leq \eta_s\}. \end{aligned} \quad (44)$$

The term $\|\mathcal{D}_v(\mathcal{D}_b(\mathbf{u}))\|_1 + \|\mathcal{D}_h(\mathcal{D}_b(\mathbf{u}))\|_1$ is the SSTV regularization. The positive value λ is a balancing parameter between the SSTV regularization and the sparse noise term. The hard constraint guarantees the ℓ_2 data-fidelity to \mathbf{v} with the radius $\varepsilon \geq 0$.³

By using the indicator function (see Eq. (6)) of $B_{2,\varepsilon}^{\mathbf{y}}$, Prob. (40) is reduced to Prob. (1) through the following reformulation:

$$\begin{aligned} \min_{\substack{\mathbf{u}, \mathbf{s}, \mathbf{l}, \\ \mathbf{z}_1, \mathbf{z}_2, \mathbf{z}_3, \mathbf{z}_4}} \quad & \iota_{B_{1,\eta_s}^{\mathbf{0}}}(\mathbf{s}) + \lambda \|\mathbf{l}\|_1 \\ & + \|\mathbf{z}_1\|_1 + \|\mathbf{z}_2\|_1 + \iota_{\{\mathbf{0}\}}(\mathbf{z}_3) + \iota_{B_{2,\varepsilon}^{\mathbf{y}}}(\mathbf{z}_4) \\ \text{s.t.} \quad & \begin{cases} \mathbf{z}_1 = \mathcal{D}_v(\mathcal{D}_b(\mathbf{u})), \\ \mathbf{z}_2 = \mathcal{D}_h(\mathcal{D}_b(\mathbf{u})), \\ \mathbf{z}_3 = \mathcal{D}_v(\mathbf{l}), \\ \mathbf{z}_4 = \mathbf{u} + \mathbf{s} + \mathbf{l}. \end{cases} \end{aligned} \quad (45)$$

³The original SSTV-regularized denoising formulation proposed in [38] incorporates an ℓ_2 data-fidelity term as a part of the objective function, whereas the formulation in (40) imposes data fidelity as an ℓ_2 -ball constraint. These two formulations are essentially the same with appropriate hyperparameters, but constrained formulation like (40) is preferred in experimental comparison and real applications because it facilitates hyperparameter settings as adopted, e.g., in Refs. [8], [19], [45]–[47]

TABLE III
THE PRECONDITIONERS BY OVDP FOR MIXED NOISE REMOVAL.

| | $\Gamma_{1,1}$ | $\Gamma_{1,2}$ | $\Gamma_{1,3}$ | $\Gamma_{2,1}$ | $\Gamma_{2,2}$ | $\Gamma_{2,3}$ | $\Gamma_{2,4}$ |
|-------|--------------------------|--------------------------|--------------------------|--------------------------|--------------------------|--------------------------|--------------------------|
| OVDP1 | $\frac{1}{33}\mathbf{I}$ | \mathbf{I} | $\frac{1}{5}\mathbf{I}$ | $\frac{1}{3}\mathbf{I}$ | $\frac{1}{3}\mathbf{I}$ | $\frac{1}{3}\mathbf{I}$ | $\frac{1}{3}\mathbf{I}$ |
| OVDP2 | $\frac{1}{9}\mathbf{I}$ | \mathbf{I} | \mathbf{I} | $\frac{1}{4}\mathbf{I}$ | $\frac{1}{4}\mathbf{I}$ | $\frac{1}{33}\mathbf{I}$ | $\frac{1}{3}\mathbf{I}$ |
| OVDP3 | $\frac{1}{33}\mathbf{I}$ | $\frac{1}{33}\mathbf{I}$ | $\frac{1}{33}\mathbf{I}$ | $\frac{1}{33}\mathbf{I}$ | $\frac{1}{33}\mathbf{I}$ | $\frac{1}{33}\mathbf{I}$ | $\frac{1}{33}\mathbf{I}$ |

Applying Algorithm 1 to Prob. (45), we can compute an optimal solution of Prob. (40). Here, since it is satisfied that $\|\mathcal{D}_v \circ \mathcal{D}_b\|_{\text{op}} \leq 4$, $\|\mathcal{D}_h \circ \mathcal{D}_b\|_{\text{op}} \leq 4$,⁴ and $\|\mathbf{I}\|_{\text{op}} = 1$, the preconditioners designed by OVDP are given in Tab. III.

2) *Experimental Results and Discussion:* For SP, μ_{SP} in (17) was set as

$$\mu_{SP} = \sqrt{39}, \quad (46)$$

because the following inequality holds due to the inequality of the operator norms of block matrices [30]:

$$\begin{aligned} & \left\| \begin{bmatrix} \mathcal{D}_v \circ \mathcal{D}_b & \mathbf{O} & \mathbf{O} \\ \mathcal{D}_h \circ \mathcal{D}_b & \mathbf{O} & \mathbf{O} \\ \mathbf{O} & \mathbf{O} & \mathcal{D}_v \\ \mathbf{I} & \mathbf{I} & \mathbf{I} \end{bmatrix} \right\|_{\text{op}}^2 \\ & \leq \|\mathcal{D}_v \circ \mathcal{D}_b\|_{\text{op}}^2 + \|\mathcal{D}_h \circ \mathcal{D}_b\|_{\text{op}}^2 + \|\mathcal{D}_v\|_{\text{op}}^2 + 3\|\mathbf{I}\|_{\text{op}}^2 \\ & < 4^2 + 4^2 + 2^2 + 3 \times 1^2 = 39, \end{aligned} \quad (47)$$

where \mathbf{O} is a zero operator.

We also derived the preconditioners in (18), for (45). Let us remark that since \mathcal{D}_v , \mathcal{D}_h , and \mathcal{D}_b in (45) are not usually implemented as explicit matrices, applying ASP to (45) is not practical in real-world applications. Let $\mathbf{x} \in \mathbb{R}^{n_1 n_2 n_3}$ be a

⁴These are derived from $\|\mathcal{D}_v\|_{\text{op}} \leq 2$, $\|\mathcal{D}_h\|_{\text{op}} \leq 2$, $\|\mathcal{D}_v\|_{\text{op}} \leq 2$ [48], and the submultiplicity of operator norms (Eq. (10))

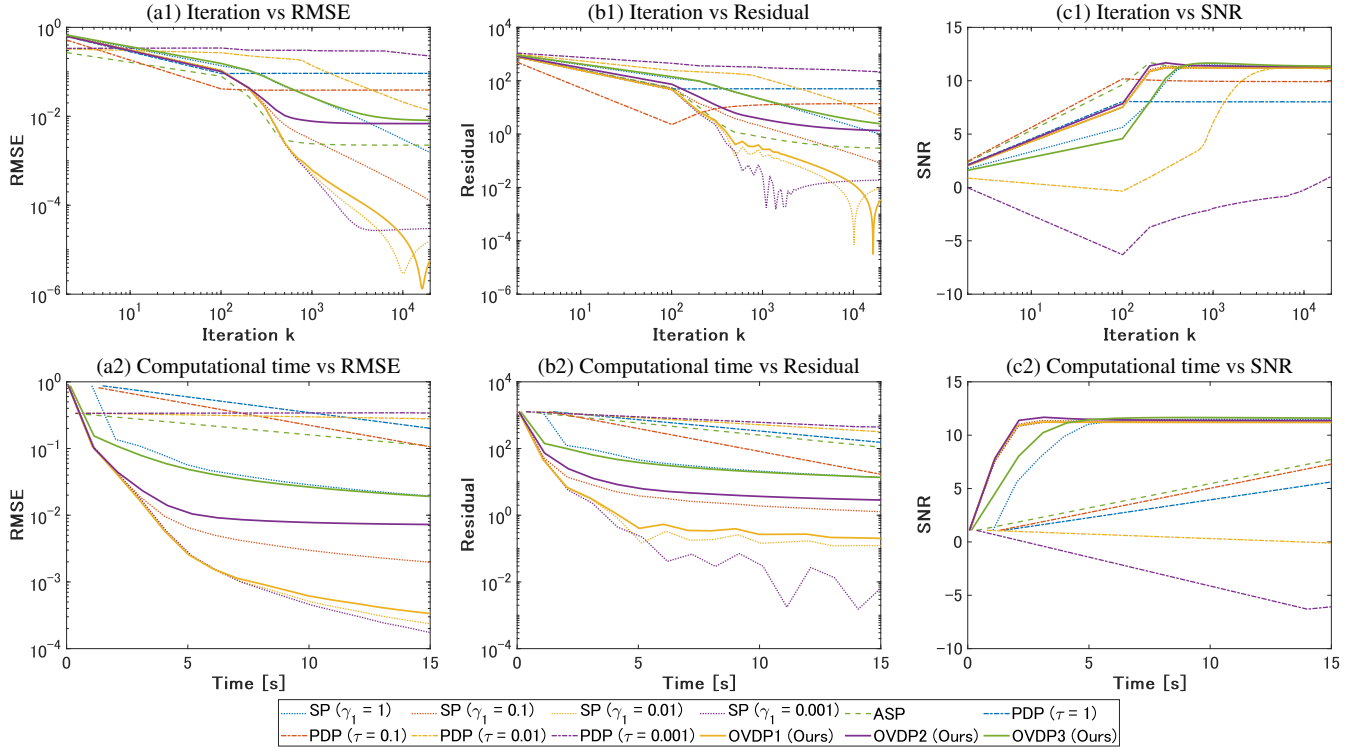


Fig. 3. Convergence profiles of the unmixing experiments. (a): Iterations/computational time versus RMSE. (b): Iterations/computational time versus Residual. (c): Iterations/computational time versus SNR.

vectorized data cube and $[\mathbf{x}]_{i_1, i_2, i_3}$ be the value of \mathbf{x} at a location (i_1, i_2, i_3) . Then the preconditioners are

$$\begin{aligned} \mathbf{\Gamma}_{1,1} &= \text{diag}(\mathbf{g}_1), \mathbf{\Gamma}_{1,2} = \mathbf{I}, \mathbf{\Gamma}_{1,3} = \text{diag}(\mathbf{g}_2), \\ \mathbf{\Gamma}_{2,1} &= \mathbf{\Gamma}_{2,2} = \frac{1}{4}, \mathbf{\Gamma}_{2,3} = \frac{1}{2}, \mathbf{\Gamma}_{2,4} = \frac{1}{3}\mathbf{I}. \end{aligned} \quad (48)$$

Here, $\mathbf{g}_1 \in \mathbb{R}^{N_1 N_2 N_3}$ and $\mathbf{g}_2 \in \mathbb{R}^{N_1 N_2 N_3}$ are given as follows:

$$[\mathbf{g}_1]_{i_1, i_2, i_3} = \begin{cases} \frac{1}{9}, & \text{if } i_1 \in I_1 \text{ and } i_2 \in E_2 \text{ and } i_3 \in I_3; \\ \frac{1}{3}, & \text{if } i_1 \in E_1 \text{ and } i_2 \in E_2 \text{ and } i_3 \in E_3; \\ \frac{1}{4}, & \text{if } i_3 \in E_3 \text{ and } \begin{cases} (i_1 \in E_1 \text{ and } i_2 \in I_2) \\ \text{or} \\ (i_1 \in I_1 \text{ and } i_2 \in E_2); \end{cases} \\ \frac{1}{5}, & \text{if } i_1 \in E_1 \text{ and } i_2 \in E_2 \text{ and } i_3 \in I_3; \\ \frac{1}{7}, & \text{otherwise,} \end{cases} \quad (49)$$

$$[\mathbf{g}_2]_{i_1, i_2, i_3} = \begin{cases} \frac{1}{3}, & \text{if } i_1 \in I_1; \\ \frac{1}{2}, & \text{otherwise,} \end{cases} \quad (50)$$

where I_m and E_m for $m = 1, 2, 3$ are $\{2, \dots, n_m - 1\}$ and $\{1, n_m\}$, respectively. In this case, the skewed proximity operators are separable and thus have analytical solutions. This indicates that P-PDS with ASP does not require FISTA.

As the ground truth HS image, we used Moffett Field [49] of size $120 \times 120 \times 176$. The observed image was generated by adding white Gaussian noise with the standard deviation $\sigma = 0.05$ and Salt & Pepper noise with the ratio $p_s = 0.1$. The parameters λ , η_s , and ε were set to 0.005, $0.5 * 0.95 * p_s * N_1 N_2 N_3$, and $0.95\sigma\sqrt{(1-p_s)N_1 N_2 N_3}$, respectively. For the

quantitative evaluation of image qualities, we used the Mean Peak Signal-to-Noise Ratio (MPSNR):

$$\text{MPSNR}(\mathbf{u}^{(t)}) := \frac{1}{N_3} \sum_{b=1}^{N_3} 10 \log_{10} \left(\frac{N_1 N_2}{\|\bar{\mathbf{u}}_b - \mathbf{u}_b^{(t)}\|_2^2} \right), \quad (51)$$

where \mathbf{u}_b is the b th band of \mathbf{u} .

Fig. 1 plots iterations versus RMSE, Residual, and MPSNR and computational time versus RMSE, Residual, and MPSNR, respectively. In terms of iterations (Figs. 1 (a1), (b1), and (c1)), P-PDSs with SP ($\gamma_1 = 0.01$), SP ($\gamma_1 = 0.001$), PDP ($\tau = 0.01$), and PDP ($\tau = 0.001$) were very slow, and P-PDSs with SP ($\gamma_1 = 1$), SP ($\gamma_1 = 0.1$), ASP, PDP ($\tau = 1$), PDP ($\tau = 0.1$), OVDP2, and OVDP3 were fast. For P-PDS with OVDP1, the evolution of the MPSNR values was slightly slow, but the convergence of the RMSE and Residual values was not. In terms of computational time (Figs. 1 (a2), (b2), and (c2)), although P-PDSs with SP, ASP, and OVDP have the same computational complexity per iteration in O -notation, P-PDS with ASP took longer than P-PDSs with SP and OVDP. When computing the analytic solutions of the proximity operators, P-PDSs with SP and OVDP require the multiplication of a scalar and a vector, while P-PDS with ASP requires the element-wise multiplication of two vectors. Since the latter takes longer to run than the former, P-PDS with ASP was longer in running time. P-PDSs with PDP were very slow because they require the iterative algorithm to calculate the skewed proximity operator.

Fig. 2 shows the denoising results and the MPSNR values [dB] obtained by P-PDS with SP ($\gamma_1 = 0.1$), ASP, PDP ($\tau = 0.1$), OVDP1, OVDP2, and OVDP3. The algorithm was

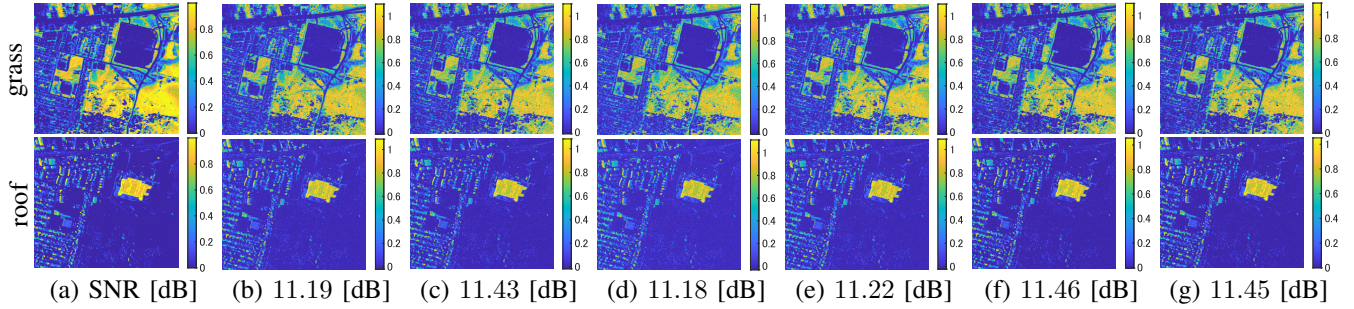


Fig. 4. Abundance maps of HS unmixing results. (a): The ground truth abundance maps. (b): The abundance maps estimated by P-PDS with SP [3] ($\gamma_1 = 0.001$). (c): The abundance maps estimated by P-PDS with ASP [15]. (d): The abundance maps estimated by P-PDS with PDP [18] ($\tau = 0.01$). (e): The abundance maps estimated by P-PDS with OVDP1 (Ours). (f): The abundance maps estimated by P-PDS with OVDP2 (Ours). (g): The abundance maps estimated by P-PDS with OVDP3 (Ours).

run until satisfying the stopping criterion or reaching 10000 iterations. We can see that all results are almost the same in terms of the MPSNR and the visual qualities.

C. Application to Hyperspectral Unmixing

An HS image is a three-dimensional data cube that consists of two-dimensional spatial information and one-dimensional spectral information. Compared to grayscale or RGB images, HS images offer more than several hundred bands, each of which contains specific unique wavelength characteristics of materials such as minerals, soils, and liquids. Due to the trade-off between spatial resolution and wavelength resolution, HS sensors do not have a sufficient spatial resolution, resulting in containing multiple components (called endmembers) in a pixel [50], which refers to as a mixel. The process of decomposing the mixels into endmembers and their abundance maps is called unmixing. Unmixing has been actively studied in the remote sensing field because of its indispensability for analyzing HS images [35], [51]. One of the popular unmixing methods is the constrained collaborative sparse regression problem [52], which has attracted attention as an optimization-based strategy for HS unmixing [53]–[55].

1) *Problem Formulation*: Let $\mathbf{v}_i \in \mathbb{R}^{N_3 \times 1}$ represent an N_3 -dimensional i th pixel vector of an HS image with N_3 spectral bands and $\mathbf{E} = [\mathbf{e}_1, \dots, \mathbf{e}_{N_e}] \in \mathbb{R}^{N_3 \times N_e}$ be an endmember matrix that denotes a spectral library with N_e spectral signatures. The pixel \mathbf{v}_i can be modeled as the following form of linear combination:

$$\mathbf{v}_i = \mathbf{E}\mathbf{a}_i + \mathbf{n}_i, \quad (52)$$

where $\mathbf{a}_i \in \mathbb{R}^{N_3 \times 1}$ is an abundance map. Introducing the extended endmember matrix $\tilde{\mathbf{E}} = \text{diag}(\mathbf{E}, \dots, \mathbf{E}) \in \mathbb{R}^{N_1 N_2 N_3 \times N_1 N_2 N_e}$, we can express an observed HS image $\mathbf{v} = [\mathbf{v}_1^\top, \dots, \mathbf{v}_{N_1 N_2}^\top]^\top$ as

$$\mathbf{v} = \tilde{\mathbf{E}}\mathbf{a} + \mathbf{n}. \quad (53)$$

Based on the above model, the constrained collaborative sparse regression problem of unmixing is formulated as the following convex optimization problem:

$$\min_{\mathbf{a}} \|\mathbf{a}\|_{1,2} \text{ s.t. } \tilde{\mathbf{E}}\mathbf{a} \in B_{2,\varepsilon}^{\mathbf{v}}, \mathbf{a} \in \mathbb{R}_+^{N_1 N_2 N_3}. \quad (54)$$

TABLE IV
THE PRECONDITIONERS BY OVDP FOR UNMIXING.

| | $\Gamma_{1,1}$ | $\Gamma_{2,1}$ | $\Gamma_{2,2}$ |
|-------|---|---|----------------|
| OVDP1 | $\frac{1}{\ \tilde{\mathbf{E}}\ _{\text{op}}^2 + 1} \mathbf{I}$ | \mathbf{I} | \mathbf{I} |
| OVDP2 | $\frac{1}{\ \tilde{\mathbf{E}}\ _{\text{op}} + 1} \mathbf{I}$ | $\frac{1}{\ \tilde{\mathbf{E}}\ _{\text{op}}} \mathbf{I}$ | \mathbf{I} |
| OVDP3 | $\frac{1}{2} \mathbf{I}$ | $\frac{1}{\ \tilde{\mathbf{E}}\ _{\text{op}}^2} \mathbf{I}$ | \mathbf{I} |

The first term is the mixed $\ell_{1,2}$ norm, which is defined by

$$\|\mathbf{a}\|_{1,2} = \sum_{\varepsilon=1}^{N_e} \sqrt{\sum_{i=1}^{N_1 N_2} [\mathbf{a}_i]_{\varepsilon}^2}. \quad (55)$$

The first constraint serves as data-fidelity with the \mathbf{v} -centered ℓ_2 -ball of the radius $\varepsilon > 0$.⁵ The second constraint enforces \mathbf{a} to belong to the nonnegative orthant $\mathbb{R}_+^{N_1 N_2 N_3}$.

By using the indicator functions (see Eq. (6)) of $B_{2,\varepsilon}^{\mathbf{v}}$ and $\mathbb{R}_+^{N_1 N_2 N_3}$, Prob. (54) is reduced to Prob. (1) via the following reformulation:

$$\begin{aligned} \min_{\mathbf{a}, \mathbf{z}_1, \mathbf{z}_2} \quad & \|\mathbf{a}\|_{1,2} + \iota_{B_{2,\varepsilon}^{\mathbf{v}}}(\mathbf{z}_1) + \iota_{\mathbb{R}_+^{N_1 N_2 N_3}}(\mathbf{z}_2) \\ \text{s.t.} \quad & \begin{cases} \mathbf{z}_1 = \tilde{\mathbf{E}}\mathbf{a}, \\ \mathbf{z}_2 = \mathbf{a}. \end{cases} \end{aligned} \quad (56)$$

Applying Algorithm 1 to Prob. (56), we can obtain an optimal solution of Prob. (54). Since the functions $\|\cdot\|_{1,2}$ and $\iota_{B_{2,\varepsilon}^{\mathbf{v}}}$ are not separable for each element of the input variable, an iterative algorithm is needed for the calculation of their skewed proximity operators relative to the metric induced by the preconditioners of ASP and PDP. Here, the preconditioners designed by OVDP are as in Tab. IV.

2) *Experimental Results and Discussion*: For SP, μ_{SP} in (17) was set as

$$\mu_{SP} = \sqrt{\|\tilde{\mathbf{E}}\|_{\text{op}}^2 + 1}, \quad (57)$$

⁵The original constrained collaborative sparse regression formulation proposed in [52] incorporates an ℓ_2 data-fidelity term as a part of the objective function, whereas the formulation in (54) imposes data fidelity as an ℓ_2 -ball constraint. The reason is similar to the case of the mixed noise removal experiment.

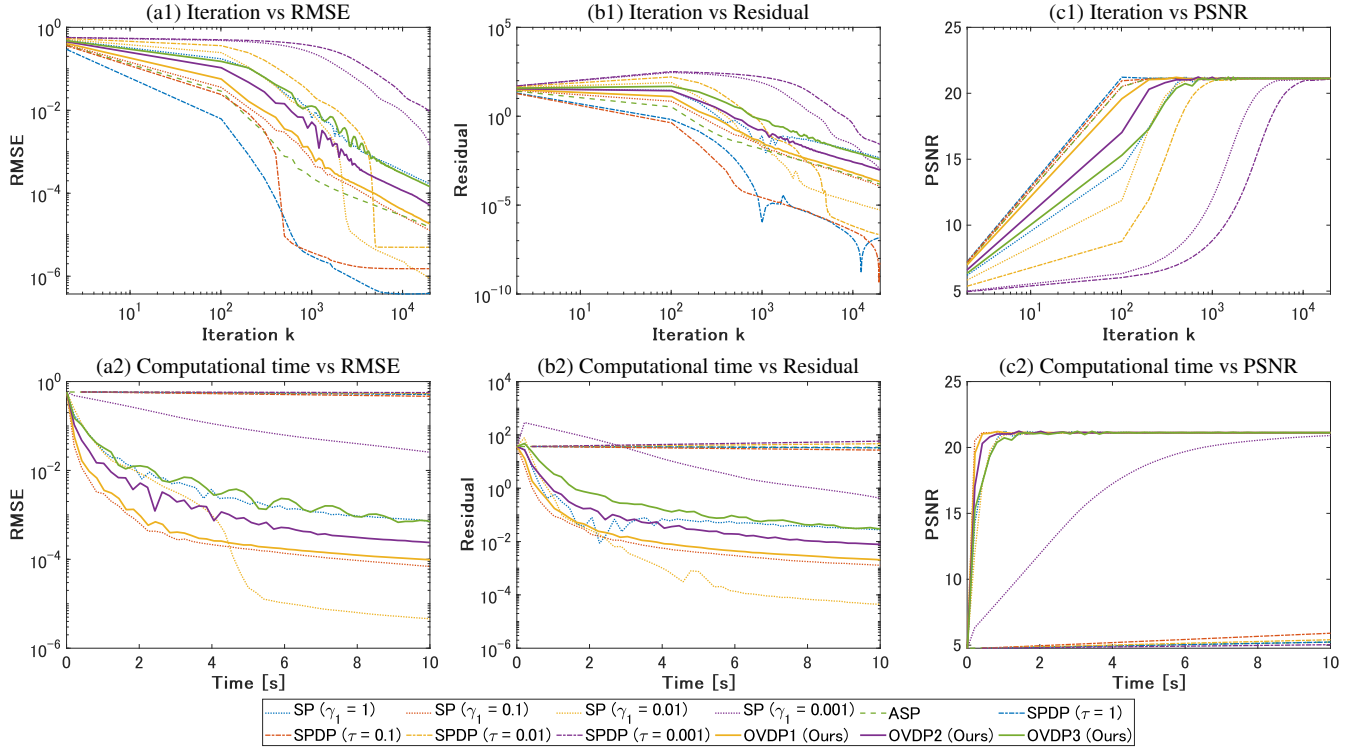


Fig. 5. Convergence profiles of the graph signal recovery experiments. (a): Iterations/computational time versus RMSE. (b): Iterations/computational time versus Residual. (c): Iterations/computational time versus PSNR.

because the following inequality holds due to the inequality of the operator norms of block matrices [30]:

$$\left\| \begin{bmatrix} \tilde{\mathbf{E}} \\ \mathbf{I} \end{bmatrix} \right\|_{\text{op}}^2 \leq \|\tilde{\mathbf{E}}\|_{\text{op}}^2 + \|\mathbf{I}\|_{\text{op}}^2 = \|\tilde{\mathbf{E}}\|_{\text{op}}^2 + 1. \quad (58)$$

For PDP, the preconditioners in (21) were used since the number of dual variables is two.

As the ground truth HS image, we used the urban dataset⁶, which has been widely used in the field of HS unmixing. The image consists of 307×307 pixels with 210 spectral bands. In the image, six main endmembers can be observed in the scene: asphalt road, grass, tree, roof, metal, and dirt. The observed data was generated by adding white Gaussian noise with the standard deviation $\sigma = 0.05$. The parameter ε was set to $0.9\sigma\sqrt{N_1N_2N_3}$. For the quantitative evaluation of image qualities, we used the Signal-to-Noise Ratio (SNR)⁷:

$$\text{SNR}(\mathbf{a}^{(t)}) := 10 \log_{10} \left(\frac{\|\bar{\mathbf{a}}\|_2}{\|\mathbf{a}^{(t)} - \bar{\mathbf{a}}\|_2} \right), \quad (59)$$

where $\mathbf{a}^{(t)}$ and $\bar{\mathbf{a}}$ are the estimated and ground true abundance maps, respectively.

Fig. 3 plots iterations versus RMSE, Residual, and SNR and computational time versus RMSE, Residual, and SNR, respectively. In terms of iterations (Figs. 3 (a1), (b1), and (c1)), P-PDS with PDP was very slow in all parameter cases. P-PDSs with SP ($\gamma_1 = 1$), OVDP2, and OVDP3 were slightly slow, but P-PDSs with SP ($\gamma_1 = 0.1$) and ASP were not. P-PDSs

with SP ($\gamma_1 = 0.01$), SP ($\gamma_1 = 0.001$), and OVDP1 were fast. In terms of computational time (Figs. 3 (a2), (b2), and (c2)), P-PDS with SP and OVDP were similar to the results with respect to iterations. P-PDSs with ASP and PDP were very slow because they require the iterative algorithm to calculate the skewed proximity operator in each iteration of P-PDS. At first glance, the curves generated by P-PDSs with PDP ($\tau = 1, 0.1$, and 0.001) may appear to converge to different SNRs. This is because they take enormous amounts of time to converge (in fact, the convergence times are too enormous to measure). Therefore, they do not converge to different SNRs.

Fig. 4 shows the unmixing results and the SNR values [dB] obtained by P-PDS with SP ($\gamma_1 = 0.001$), ASP, PDP ($\tau = 0.01$), OVDP1, OVDP2, and OVDP3. The algorithm was run until satisfying the stopping criterion or reaching 10000 iterations. We can see that all results are almost the same in terms of the SNR and the visual qualities.

D. Application to Graph Signal Recovery

Graphs explicitly represent the irregular structures of data [56]–[58], such as traffic and sensor network data, geographical data, mesh data, and biomedical data. The signals on the irregular structures are called graph signals. Similar to classical signal processing, sampling of graph signals [59] is a leading research topic due to its numerous promising applications, for example, sensor placement, filter bank designs, traffic monitoring, and semi-supervised learning. In graph signal recovery, which reconstructs original graph signals from sampled graph signals, it is assumed that graph signals have some properties, such as smoothness. The smoothness of

⁶<http://www.tec.army.mil/Hypercube>

⁷This evaluation metric is often referred to as the signal to reconstruction error in the literature of HS unmixing (e.g., [52], [54], [55]).

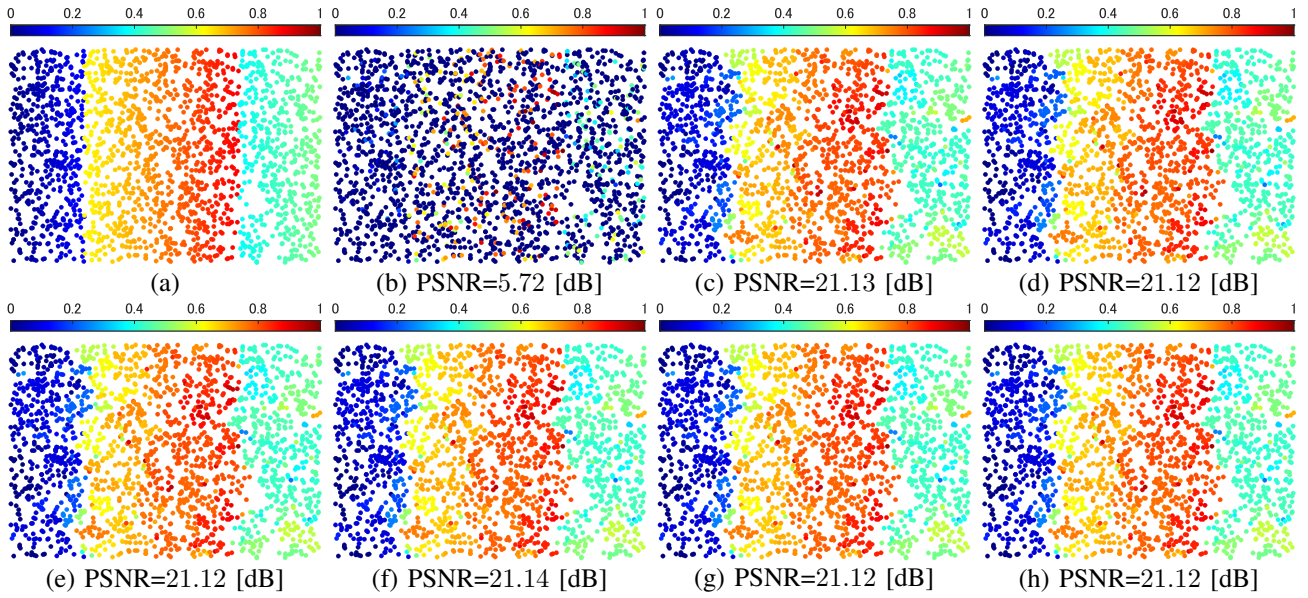


Fig. 6. Graph signal recovery results. (a): The ground truth signal. (b): The observed graph signal. (c): The graph signal estimated by P-PDS with SP [3] ($\gamma_1 = 0.1$). (d): The graph signal estimated by P-PDS with ASP [15]. (e): The graph signal estimated by P-PDS with PDP [18] ($\tau = 1$). (f): The graph signal estimated by P-PDS with OVDP1 (Ours). (g): The graph signal estimated by P-PDS with OVDP2 (Ours). (h): The graph signal estimated by P-PDS with OVDP3 (Ours).

graph signals can be captured by graph total variation type regularizations [60]–[62], which have been applied to various graph signal processing tasks [63], [64].

1) *Problem Formulation:* We consider signals on weighted directed graphs $\mathcal{G} = (\mathcal{V}, \mathcal{E}, \mathbf{W})$ with a vertex set $\mathcal{V} = \{1, \dots, N_{\mathcal{G}}\}$, an edge set $\mathcal{E} \subseteq \mathcal{V} \times \mathcal{V}$, and a weighted matrix $\mathbf{W} \in \mathbb{R}^{N_{\mathcal{G}} \times N_{\mathcal{G}}}$. The value $W_{i,j}$ is designed to be large if the relation between vertices i and j is strong. Graph signals are typically assumed to be smooth with respect to the graph \mathcal{G} . Based on the assumption, graph signal recovery methods often adopt the graph total variation (GTV) [57], [62]:

$$\|\mathbf{x}\|_{\text{GTV}} := \|\mathbf{D}_{\mathcal{G}}\mathbf{x}\|_{1,2} = \sum_{i=1}^{N_{\mathcal{G}}} \|\mathbf{y}_i\|_2, \quad (60)$$

where $\mathbf{D}_{\mathcal{G}}$ is the graph difference operator defined as follows. Let $\mathbf{D}_{\mathcal{G}}\mathbf{x} = [\mathbf{y}_1^\top, \dots, \mathbf{y}_{N_{\mathcal{G}}}^\top]$, then each \mathbf{y}_i consists of the weighted differences between the graph signal value x_i at an i th vertex and the graph signal values x_j ($\forall j \in \mathcal{N}(i) := \{k \in \mathcal{V} \mid W_{i,k} \neq 0\}$) at its connected vertices $\mathcal{N}(i)$, i.e.,

$$[\mathbf{y}_i]_j := (x_j - x_i)W_{i,j}, \quad (\forall j \in \mathcal{N}(i)). \quad (61)$$

By weighting the difference between x_i and x_j by $W_{i,j}$, GTV can capture the graph signal smoothness that the difference of graph signal values is small as the relation of their vertices is strong.

Consider that an observed graph signal $\mathbf{v} \in \mathbb{R}^{M_{\mathcal{G}}}$ is modeled by

$$\mathbf{v} = \Phi \bar{\mathbf{u}} + \mathbf{n}, \quad (62)$$

where $\bar{\mathbf{u}} \in \mathbb{R}^{N_{\mathcal{G}}}$, $\mathbf{n} \in \mathbb{R}^{M_{\mathcal{G}}}$, and $\Phi \in \{0, 1\}^{M_{\mathcal{G}} \times N_{\mathcal{G}}}$ are the true graph signal of interest, random additive noise, and the sampling matrix, respectively. Based on this observation

TABLE V
THE PRECONDITIONERS BY OVDP FOR GRAPH SIGNAL RECOVERY.

| | $\Gamma_{1,1}$ | $\Gamma_{2,1}$ | $\Gamma_{2,2}$ |
|-------|---|---|----------------|
| OVDP1 | $\frac{1}{\ \mathbf{D}_{\mathcal{G}}\ _{\text{op}}^2 + 1} \mathbf{I}$ | \mathbf{I} | \mathbf{I} |
| OVDP2 | $\frac{1}{\ \mathbf{D}_{\mathcal{G}}\ _{\text{op}} + 1} \mathbf{I}$ | $\frac{1}{\ \mathbf{D}_{\mathcal{G}}\ _{\text{op}}} \mathbf{I}$ | \mathbf{I} |
| OVDP3 | $\frac{1}{2} \mathbf{I}$ | $\frac{1}{\ \mathbf{D}_{\mathcal{G}}\ _{\text{op}}^2} \mathbf{I}$ | \mathbf{I} |

model, the GTV regularized graph signal recovery problem is formulated as the following convex optimization problem [62]:

$$\min_{\mathbf{u}} \|\mathbf{D}_{\mathcal{G}}\mathbf{u}\|_{\text{GTV}} \text{ s.t. } \Phi \mathbf{u} \in B_{2,\varepsilon}^{\mathbf{y}}. \quad (63)$$

The hard constraint guarantees the ℓ_2 data fidelity to the observed signal \mathbf{v} with the radius ε .

By using the indicator function (see Eq. (6)) of $B_{2,\varepsilon}^{\mathbf{y}}$, Prob. (63) is reduced to Prob. (1) via the following reformulation:

$$\begin{aligned} \min_{\mathbf{u}, \mathbf{z}_1, \mathbf{z}_2} \quad & \|\mathbf{z}_1\|_{1,2} + \iota_{B_{2,\varepsilon}^{\mathbf{y}}}(\mathbf{z}_2) \\ \text{s.t.} \quad & \begin{cases} \mathbf{z}_1 = \mathbf{D}_{\mathcal{G}}\mathbf{u}, \\ \mathbf{z}_2 = \Phi \mathbf{u}. \end{cases} \end{aligned} \quad (64)$$

Applying Algorithm 1 to Prob. (64), we can compute an optimal solution of Prob. (63). Since the function $\|\cdot\|_{1,2}$ is not separable for each element of the input variable, an iterative algorithm is needed for the computation of their skewed proximity operators relative to the metric induced by the preconditioners of ASP and PDP in (18). Here, the preconditioners designed by OVDP are given as in Tab. V. According to [62], an upper bound of the operator norm

TABLE VI

THE NUMBER OF ITERATIONS TO MEET THE STOPPING CRITERIA. XXX* MEANS THAT THE METHOD REQUIRES MORE THAN XXX ITERATIONS.

| | Methods | | | | | | | | | | | |
|-----------------------|--------------------|----------------------|-----------------------|------------------------|------|----------------|------------------|-------------------|--------------------|-------|-------|-------|
| | SP | | | | ASP | PDP | | | | OVDPI | OVDP2 | OVDP3 |
| | ($\gamma_1 = 1$) | ($\gamma_1 = 0.1$) | ($\gamma_1 = 0.01$) | ($\gamma_1 = 0.001$) | | ($\tau = 1$) | ($\tau = 0.1$) | ($\tau = 0.01$) | ($\tau = 0.001$) | | | |
| Mixed noise removal | 10000* | 4736 | 10000* | 10000* | 3323 | 10000* | 1552 | 10000* | 10000* | 5470 | 3325 | 9755 |
| Unmixing | 2943 | 395 | 350 | 349 | 300 | 10000* | 10000* | 10000* | 10000* | 350 | 525 | 4709 |
| Graph signal recovery | 3625 | 806 | 1937 | 10000* | 448 | 194 | 396 | 4129 | 10000* | 998 | 1846 | 3546 |
| Average | 5523* | 1979 | 4096* | 6783* | 1357 | 6731* | 3983* | 8043* | 10000* | 2273 | 1899 | 6003 |

TABLE VII

RUNNING TIME [S] TO MEET THE STOPPING CRITERIA. XXX* MEANS THAT THE METHOD REQUIRES MORE THAN XXX [S].

| | Methods | | | | | | | | | | | |
|-----------------------|--------------------|----------------------|-----------------------|------------------------|--------|----------------|------------------|-------------------|--------------------|--------|-------|--------|
| | SP | | | | ASP | PDP | | | | OVDPI | OVDP2 | OVDP3 |
| | ($\gamma_1 = 1$) | ($\gamma_1 = 0.1$) | ($\gamma_1 = 0.01$) | ($\gamma_1 = 0.001$) | | ($\tau = 1$) | ($\tau = 0.1$) | ($\tau = 0.01$) | ($\tau = 0.001$) | | | |
| Mixed noise removal | 1000* | 111.86 | 333.72 | 1000* | 230.40 | 1000* | 1000* | 1000* | 1000* | 130.70 | 79.35 | 231.78 |
| Unmixing | 3.52 | 3.97 | 3.60 | 3.60 | 64.44 | 1000* | 1000* | 1000* | 1000* | 11.38 | 5.44 | 46.13 |
| Graph signal recovery | 7.54 | 1.65 | 4.00 | 40.61 | 1000* | 607.90 | 450.60 | 1000* | 1000* | 2.04 | 3.73 | 7.21 |

$\|\mathbf{D}_{\mathcal{G}}\|_{\text{op}}$ can be derived by

$$\|\mathbf{D}_{\mathcal{G}}\|_{\text{op}} \leq 2 \max_{i \in \mathcal{V}} \sum_{j \in \mathcal{V}} (W_{i,j}^2 + W_{j,i}^2). \quad (65)$$

An upper bound of the norm of the sampling matrix is one, i.e., $\|\Phi\|_{\text{op}} = 1$.

2) *Experimental Results:* For SP, μ_{SP} in (17) was set as

$$\mu_{SP} = \sqrt{\|\mathbf{D}_{\mathcal{G}}\|_{\text{op}}^2 + 1}, \quad (66)$$

because the following inequality holds due to the inequality of the operator norms of block matrices [30]:

$$\left\| \begin{bmatrix} \mathbf{D}_{\mathcal{G}} \\ \Phi \end{bmatrix} \right\|_{\text{op}}^2 \leq \|\mathbf{D}_{\mathcal{G}}\|_{\text{op}}^2 + \|\Phi\|_{\text{op}}^2 \leq \|\mathbf{D}_{\mathcal{G}}\|_{\text{op}}^2 + 1. \quad (67)$$

The preconditioners by ASP in (18) for Prob. (63) are

$$\begin{aligned} [\mathbf{F}_{1,1}]_{i,i} &= \frac{1}{\sum_{j=1}^{N_{\mathcal{G}}N_{\mathcal{G}}} |W_{i,j}| + \sum_{k=1}^{M_{\mathcal{G}}} \Phi_{k,i}}, \quad (\forall i = 1, \dots, N_{\mathcal{G}}), \\ [\mathbf{F}_{2,1}]_{i,i} &= \frac{1}{2 \sum_{j=1}^{N_{\mathcal{G}}} |W_{j,i}|}, \quad (\forall i = 1, \dots, N_{\mathcal{G}}N_{\mathcal{G}}), \\ [\mathbf{F}_{2,2}]_{i,i} &= 1, \quad (\forall i = 1, \dots, M_{\mathcal{G}}). \end{aligned} \quad (68)$$

For PDP, the preconditioners in (21) were used since the number of dual variables is two.

We constructed a random sensor graph \mathcal{G} by using GSP-Box [65], then generated a noiseless piece-wise smooth graph signal on the graph with $N_{\mathcal{G}} = 2000$ vertices. The observed graph signal was obtained by adding white Gaussian noise with 0.1 of the standard deviation σ and by sampling it with 0.2 of the sampling rate ($M_{\mathcal{G}} = 0.2N_{\mathcal{G}}$). The parameter ε was set as $\varepsilon = 0.9\sigma\sqrt{M_{\mathcal{G}}}$. For the quantitative evaluation of recovery qualities, we used the Peak Signal-to-Noise Ratio (PSNR):

$$\text{PSNR} := 10 \log_{10} \left(\frac{N_{\mathcal{G}}}{\|\bar{\mathbf{u}} - \mathbf{u}^{(t)}\|_2^2} \right), \quad (69)$$

Fig. 5 plots iterations versus RMSE, Residual, and PSNR and computational time versus RMSE, Residual, and PSNR, respectively. In terms of iterations (Figs. 5 (a1), (b1), and (c1)),

P-PDSs with SP ($\gamma_1 = 0.001$) and PDP ($\tau = 0.001$) were very slow. P-PDSs with SP ($\gamma_1 = 1$), PDP ($\tau = 0.01$), OVDPI, OVDP2, and OVDP3 were not slow but not fast. P-PDSs with SP ($\gamma_1 = 0.1$), SP ($\gamma_1 = 0.01$), ASP, PDP ($\tau = 1$), PDP ($\tau = 0.1$), OVDPI, and OVDP2 were fast. In terms of computational time (Figs. 5 (a2), (b2), and (c2)), P-PDS with SP and OVDP were similar to the results with respect to iterations. P-PDSs with ASP and PDP were very slow because they require the iterative algorithm to calculate the skewed proximity operator.

Fig. 6 shows the recovery results and the PSNR values [dB] obtained by P-PDS with SP ($\gamma_1 = 0.1$), ASP, PDP ($\tau = 1$), OVDPI, OVDP2, and OVDP3. The algorithm was run until satisfying the stopping criterion or reaching 10000 iterations. We can see that all results are almost the same in terms of the PSNR and the visual qualities.

E. Discussion

For discussion based on numerical values, we compare the number of iterations (Tab. VI) and running time (Tab. VII) to satisfy the stopping criteria in Tab. II.

The appropriate parameter for SP (γ_1) varied depending on the optimization problem and were 0.1 for mixed noise removal, 0.01 and 0.001 for unmixing, and 0.1 and 0.01 for graph signal recovery. If γ_1 is adjusted appropriately, as in the case of the unmixing experiments ($\gamma_1 = 0.01$ and 0.001), P-PDS with SP can converge faster than the automatic preconditioner design methods (ASP and OVDP). However, no parameter results in fast convergence for any optimization problem, and the convergence might be extremely slow, such as at 0.01 and 0.001 for mixed noise removal, at 1 for unmixing, and at 0.001 for graph signal recovery. Therefore, γ_1 needs to be manually adjusted according to each problem.

P-PDS with ASP was the best in terms of the average number of iterations, and P-PDS with PDP (τ is adjusted) resulted in a small number of iterations to converge for both graph signal recovery and mixed noise removal. However, for the unmixing experiments, P-PDS with PDP required a more significant number of iterations to converge than P-PDS with SP ($\gamma_1 = 0.01$ and 0.001) and OVDP. We speculate

that this is because the optimization problem of unmixing is relatively complicated; it involves an endmember matrix, while the optimization problems of mixed noise removal and graph signal recovery only include relatively simple difference operators and random sampling matrices in their optimization problems. Although P-PDSs with ASP and PDP were fast in the number of iterations, they took a much longer running time to converge. This is due to the fact that they require iterative algorithms such as FISTA to compute the skewed proximity operator in each iteration of P-PDS. Incidentally, since the internal iterations of FISTA vary depending on the task and parameters (e.g., τ), the execution time of P-PDS may be long relative to the number of iterations to convergence. For example, P-PDS with PDP ($\tau = 1$) required fewer iterations but a longer running time than P-PDS with PDP ($\tau = 0.1$). In addition, P-PDS with ASP took a very long running time per iteration in the graph signal recovery experiment, while it took a short running time in the unmixing experiments.

P-PDSs with OVDP achieved good convergence speed in both the number of iterations and the running time thanks to a diagonal preconditioning technique based on the problem structure. In addition, they maintain the proximability of the functions, resulting in fast running time. P-PDS with OVDP2 was fast on average in the number of iterations. Moreover, P-PDS with OVDP2 produced the fastest result in terms of running time for the mixed noise removal experiment. P-PDS with OVDP1 was faster than P-PDS with OVDP2 and OVDP3 for the unmixing and graph signal recovery experiments. Furthermore, the preconditioners of OVDP can be easily calculated in the mixed noise removal case whose optimization problem incorporates the linear operators implemented not as explicit matrices.

These results indicate the following conclusions.

- SP and PDP are effective for cases where preconditioners are easily adjusted. In particular, PDP is very effective for the cases where the structure of an optimization problem is simple and the calculation of an inner iteration is efficient.
- ASP is applicable to the cases where the structure of an optimization problem is simple, the calculation of an inner iteration is efficient, and the optimization problem only contains linear operators implemented as the represented matrix.
- Our OVDP can determine effective preconditioners regardless of whether or not the above conditions are satisfied. Specifically, for the signal estimation problem that can be handled by ASP, our OVDP was several hundred times faster than ASP.
- In addition, P-PDS with our OVDP required fewer iterations on average than P-PDSs with SP or PDP, which require manual adjustments.

V. CONCLUSION

We have proposed OVDP, which automatically and easily designs preconditioners in a variable-wise manner when a given optimization problem incorporates linear operators represented not as explicit matrices. We also proved the convergence of P-PDS with OVDP. Applications of our method

to three signal estimation tasks have been provided with experimental comparison, where we have shown that our method achieved the fast convergence speed on average and raised the examples of signal processing tasks that OVDP is effective to be applied.

APPENDIX PROOF OF LEMMA III.1

Proof. Let r be the rank of \mathbf{A} and $\sigma_1(\mathbf{A}), \dots, \sigma_r(\mathbf{A})$ be the singular values of \mathbf{A} . Then, \mathbf{A} can be decomposed as

$$\mathbf{A} = \mathbf{U}\mathbf{\Sigma}\mathbf{V}^*, \quad (70)$$

where $\mathbf{U} \in \mathbb{R}^{m \times r}$ and $\mathbf{V} \in \mathbb{R}^{n \times r}$ satisfy $\mathbf{U}^*\mathbf{U} = \mathbf{I}$ and $\mathbf{V}^*\mathbf{V} = \mathbf{I}$. Then, we introduce an $r \times r$ unitary matrix \mathbf{W} and define \mathbf{B} and \mathbf{C} as

$$\mathbf{B} = \mathbf{U}\mathbf{\Sigma}^{1-\beta}\mathbf{W}^*, \mathbf{C} = \mathbf{W}\mathbf{\Sigma}^\beta\mathbf{V}^*, \quad (71)$$

where $\mathbf{\Sigma}^{1-\beta} = \text{diag}(\sigma_1(\mathbf{A})^{1-\beta}, \dots, \sigma_r(\mathbf{A})^{1-\beta})$ and $\mathbf{\Sigma}^\beta = \text{diag}(\sigma_1(\mathbf{A})^\beta, \dots, \sigma_r(\mathbf{A})^\beta)$. It is clear that $\mathbf{A} = \mathbf{B}\mathbf{C}$. In turn, we obtain from the definition that

$$\begin{aligned} \|\mathbf{B}\mathbf{x}\|_2^2 &= \|\mathbf{\Sigma}^{1-\beta}\mathbf{W}^*\mathbf{x}\|_2^2 \\ &\leq \sigma_1(\mathbf{A})^{2-2\beta} \|\mathbf{W}^*\mathbf{x}\|_2^2 \\ &= \sigma_1(\mathbf{A})^{2-2\beta} \|\mathbf{x}\|_2^2. \end{aligned} \quad (72)$$

Hence

$$\|\mathbf{B}\|_{\text{op}} = \sup_{\mathbf{x} \neq \mathbf{0}} \frac{\|\mathbf{B}\mathbf{x}\|_2}{\|\mathbf{x}\|_2} = \sigma_1(\mathbf{A})^{1-\beta}. \quad (73)$$

Arguing similarly, \mathbf{C} satisfies $\|\mathbf{C}\|_{\text{op}} = \sigma_1(\mathbf{A})^\beta$. □

REFERENCES

- [1] N. Parikh and S. Boyd, "Proximal algorithms," *Found. Trends Mach. Learn.*, vol. 1, no. 3, pp. 127–239, 2014.
- [2] P. L. Combettes and J.-C. Pesquet, "Fixed point strategies in data science," *IEEE Trans. Signal Process.*, vol. 69, pp. 3878–3905, 2021.
- [3] A. Chambolle and T. Pock, "A first-order primal-dual algorithm for convex problems with applications to imaging," *J. Math. Imag. Vis.*, vol. 40, no. 1, pp. 120–145, 2010.
- [4] L. Condat, "A generic proximal algorithm for convex optimization—application to total variation minimization," *IEEE Signal Process. Lett.*, vol. 21, no. 8, pp. 985–989, Aug. 2014.
- [5] T. Goldstein, M. Li, and X. Yuan, "Adaptive primal-dual splitting methods for statistical learning and image processing," in *Proc. Advances Neural Inf. Process. Syst.*, C. Cortes, N. Lawrence, D. Lee, M. Sugiyama, and R. Garnett, Eds., vol. 28. Curran Associates, Inc., 2015, pp. 2089–2097. [Online]. Available: <https://proceedings.neurips.cc/paper/2015/file/cd758e8f59dfdf06a852adad277986ca-Paper.pdf>
- [6] S. Ono and I. Yamada, "Hierarchical convex optimization with primal-dual splitting," *IEEE Trans. Signal Process.*, vol. 63, no. 2, pp. 373–388, Jan. 2015.
- [7] N. Komodakis and J.-C. Pesquet, "Playing with duality: An overview of recent primal-dual approaches for solving large-scale optimization problems," *IEEE Signal Process. Mag.*, vol. 32, no. 6, pp. 31–54, Nov. 2015.
- [8] S. Ono, "Primal-dual plug-and-play image restoration," *IEEE Signal Process. Lett.*, vol. 24, no. 8, pp. 1108–1112, Aug. 2017.
- [9] Y. Malitsky and T. Pock, "A first-order primal-dual algorithm with linesearch," *SIAM J. Optim.*, vol. 28, no. 1, pp. 411–432, 2018.
- [10] S. Kyoichi, S. Ono, and I. Selesnick, "Epigraphical relaxation for minimizing layered mixed norms," *IEEE Trans. Signal Process.*, vol. 69, pp. 2923–2938, 2021.
- [11] B. He, F. Ma, S. Xu, and X. Yuan, "A generalized primal-dual algorithm with improved convergence condition for saddle point problems," *SIAM J. Imag. Sci.*, vol. 15, no. 3, pp. 1157–1183, 2022.

- [12] X.-K. Chang, J. Yang, and H. Zhang, "Golden ratio primal-dual algorithm with linesearch," *SIAM J. Optim.*, vol. 32, no. 3, pp. 1584–1613, 2022.
- [13] L. Condat, "A primal-dual splitting method for convex optimization involving lipschitzian, proximable and linear composite terms," *J. Opt. Theory Appl.*, vol. 158, no. 2, pp. 460–479, 2013.
- [14] B. C. Vu, "A splitting algorithm for dual monotone inclusions involving cocoercive operators," *Adv. Comput. Math.*, vol. 38, no. 3, pp. 667–681, 2013.
- [15] T. Pock and A. Chambolle, "Diagonal preconditioning for first order primal-dual algorithms in convex optimization," in *IEEE Int. Conf. Comput. Vis. (ICCV)*, Nov. 2011, pp. 1762–1769.
- [16] M. Wen, J. Peng, C. Zhu, S. Yue, and Y. Tang, "A preconditioning technique for first-order primal-dual splitting method in convex optimization," *Math. Problems Eng.*, vol. 2017, 2017. [Online]. Available: <https://www.hindawi.com/journals/mpe/2017/3694525/>
- [17] Z. Ye, T. Möllenhoff, T. Wu, and D. Cremers, "Optimization of graph total variation via active-set-based combinatorial reconditioning," in *Proc. 23rd Int. Conf. Artif. Intell. Statist.*, ser. Proceedings of Machine Learning Research, S. Chiappa and R. Calandra, Eds., vol. 108. PMLR, 26–28 Aug. 2020, pp. 657–668. [Online]. Available: <https://proceedings.mlr.press/v108/ye20a.html>
- [18] Y. Liu, Y. Xu, and W. Yin, "Acceleration of primal–dual methods by preconditioning and simple subproblem procedures," *J. Sci. Comput.*, vol. 86, no. 21, pp. 1–34, Jan. 2021.
- [19] S. Ono and I. Yamada, "Signal recovery with certain involved convex data-fidelity constraints," *IEEE Trans. Signal Process.*, vol. 63, no. 22, pp. 6149–6163, Nov. 2015.
- [20] P. L. Combettes and B. C. Vv, "Variable metric quasi-fejér monotonicity," *Nonlin. Anal.*, vol. 78, pp. 17–31, Feb. 2013. [Online]. Available: <https://www.sciencedirect.com/science/article/pii/S0362546X12003616>
- [21] S. Becker, J. Fadili, and P. Ochs, "On quasi-Newton forward-backward splitting: Proximal calculus and convergence," *SIAM J. Optim.*, vol. 29, no. 4, pp. 2445–2481, 2019. [Online]. Available: <https://doi.org/10.1137/18M1167152>
- [22] A. Chambolle, V. Caselles, D. Cremers, M. Novaga, and T. Pock, "An introduction to total variation for image analysis," in *Theoretical foundations and numerical methods for sparse recovery*. de Gruyter, 2010, pp. 263–340.
- [23] K. Bredies and M. Holler, "Higher-order total variation approaches and generalisations," *Inverse Problems*, vol. 36, no. 12, p. 123001, Dec. 2020. [Online]. Available: <https://doi.org/10.1088/1361-6420/ab8f80>
- [24] J. Kovacevic and A. Chebira, "Life beyond bases: The advent of frames (part I)," *IEEE Signal Process. Mag.*, vol. 24, no. 4, pp. 86–104, Jul. 2007.
- [25] J.-F. Cai, H. Ji, Z. Shen, and G.-B. Ye, "Data-driven tight frame construction and image denoising," *Appl. Comput. Harmon. Anal.*, vol. 37, no. 1, pp. 89–105, 2014.
- [26] A. Parekh and I. W. Selesnick, "Convex denoising using non-convex tight frame regularization," *IEEE Signal Process. Lett.*, vol. 22, no. 10, pp. 1786–1790, Oct. 2015.
- [27] G. Chierchia, E. Chouzenoux, P. L. Combettes, and J.-C. Pesquet, "The proximity operator repository," *User's guide <http://proximityoperator.net/download/guide.pdf>* (accessed October 3rd, 2021), 2020.
- [28] K. Naganuma and S. Ono, "Operator-norm-based variable-wise diagonal preconditioning for automatic stepsize selection of a primal-dual splitting algorithm," in *Proc. Eur. Signal Process. Conf. (EUSIPCO)*, Aug. 2022, pp. 2041–2045.
- [29] P. L. Combettes and N. N. Reyes, "Moreau's decomposition in banach spaces," *Math. Program.*, vol. 139, pp. 103–114, Jun. 2013.
- [30] R. Bhatia and F. Kittaneh, "Norm inequalities for partitioned operators and an application," *Math. Ann.*, vol. 287, no. 4, pp. 719–726, 1990.
- [31] A. Beck and T. M., "A fast iterative shrinkage-thresholding algorithm for linear inverse problems," *SIAM J. Imag. Sci.*, vol. 2, no. 1, pp. 183–202, 2009.
- [32] Y.-B. Zheng, T.-Z. Huang, X.-L. Zhao, T.-X. Jiang, T.-H. Ma, and T.-Y. Ji, "Mixed noise removal in hyperspectral image via low-fibered-rank regularization," *IEEE Trans. Geosci. Remote Sens.*, vol. 58, no. 1, pp. 734–749, Jan. 2020.
- [33] Y.-B. Zheng, T.-Z. Huang, X.-L. Zhao, Y. Chen, and W. He, "Double-factor-regularized low-rank tensor factorization for mixed noise removal in hyperspectral image," *IEEE Trans. Geosci. Remote Sens.*, vol. 58, no. 12, pp. 8450–8464, Dec. 2020.
- [34] L. Zhang, Y. Qian, J. Han, P. Duan, and P. Ghamisi, "Mixed noise removal for hyperspectral image with l_0 - l_1 - l_2 sstv regularization," *IEEE J. Sel. Topics Appl. Earth Observ. Remote Sens.*, vol. 15, pp. 5371–5387, Jun. 2022.
- [35] P. Ghamisi, N. Yokoya, J. Li, W. Liao, S. Liu, J. Plaza, B. Rasti, and A. Plaza, "Advances in hyperspectral image and signal processing: A comprehensive overview of the state of the art," *IEEE Geosci. Remote Sens. Mag.*, vol. 5, no. 4, pp. 37–78, 2017.
- [36] N. Audebert, B. Le Saux, and S. Lefevre, "Deep learning for classification of hyperspectral data: A comparative review," *IEEE Geosci. Remote Sens. Mag.*, vol. 7, no. 2, pp. 159–173, 2019.
- [37] H. Su, Z. Wu, H. Zhang, and Q. Du, "Hyperspectral anomaly detection: A survey," *IEEE Geosci. Remote Sens. Mag.*, vol. 10, no. 1, pp. 64–90, 2022.
- [38] H. K. Aggarwal and A. Majumdar, "Hyperspectral image denoising using spatio-spectral total variation," *IEEE Geosci. Remote Sens. Lett.*, vol. 13, no. 3, pp. 442–446, Feb. 2016.
- [39] H. Fan, C. Li, Y. Guo, G. Kuang, and J. Ma, "Spatial-spectral total variation regularized low-rank tensor decomposition for hyperspectral image denoising," *IEEE Trans. Geosci. Remote Sens.*, vol. 56, no. 10, pp. 6196–6213, Oct. 2018.
- [40] W. He, H. Zhang, H. Shen, and L. Zhang, "Hyperspectral image denoising using local low-rank matrix recovery and global spatial-spectral total variation," *IEEE J. Sel. Topics Appl. Earth Observ. Remote Sens.*, vol. 11, no. 3, pp. 713–729, Mar. 2018.
- [41] T. Ince, "Hyperspectral image denoising using group low-rank and spatial-spectral total variation," *IEEE Access*, vol. 7, pp. 52095–52109, Apr. 2019.
- [42] M. Wang, Q. Wang, J. Chanussot, and D. Hong, " l_0 - l_1 hybrid total variation regularization and its applications on hyperspectral image mixed noise removal and compressed sensing," *IEEE Trans. Geosci. Remote Sens.*, vol. 59, no. 9, pp. 7695–7710, Sep. 2021.
- [43] K. Naganuma and S. Ono, "A general destriping framework for remote sensing images using flatness constraint," *IEEE Trans. Geosci. and Remote Sens.*, vol. 60, pp. 1–16, Feb. 2022, Art no. 5525016.
- [44] S. Takemoto, K. Naganuma, and S. Ono, "Graph spatio-spectral total variation model for hyperspectral image denoising," *IEEE Geoscience and Remote Sensing Letters*, vol. 19, pp. 1–5, Jul. 2022, Art no. 6012405.
- [45] M. Afonso, J. Bioucas-Dias, and M. Figueiredo, "An augmented Lagrangian approach to the constrained optimization formulation of imaging inverse problems," *IEEE Trans. Image Process.*, vol. 20, no. 3, pp. 681–695, Mar. 2011.
- [46] G. Chierchia, N. Pustelnik, J.-C. Pesquet, and B. Pesquet-Popescu, "Epigraphical projection and proximal tools for solving constrained convex optimization problems," *Signal, Image Video Process.*, vol. 9, no. 8, pp. 1737–1749, 2015.
- [47] S. Ono, "Efficient constrained signal reconstruction by randomized epigraphical projection," in *Proc. IEEE Int. Conf. Acoust., Speech Signal Process. (ICASSP)*. IEEE, 2019, pp. 4993–4997.
- [48] A. Chambolle, "An algorithm for total variation minimization and applications," *J. Math. Imag. Vis.*, vol. 20, pp. 89–97, 2004.
- [49] "AVIRIS," https://aviris.jpl.nasa.gov/data/free_data.html.
- [50] N. Keshava and J. F. Mustard, "Spectral unmixing," *IEEE Signal Process. Mag.*, vol. 19, no. 1, pp. 44–57, 2002.
- [51] W. Ma, J. M. Bioucas-Dias, T. Chan, N. Gillis, P. Gader, A. Plaza, A. Ambikapathi, and C. Chi, "A signal processing perspective on hyperspectral unmixing: Insights from remote sensing," *IEEE Signal Process. Mag.*, vol. 31, no. 1, pp. 67–81, 2013.
- [52] M.-D. Iordache, J. M. Bioucas-Dias, and A. Plaza, "Collaborative sparse regression for hyperspectral unmixing," *IEEE Trans. Geosci. Remote Sens.*, vol. 52, no. 1, pp. 341–354, Jan. 2013.
- [53] H. K. Aggarwal and A. Majumdar, "Hyperspectral unmixing in the presence of mixed noise using joint-sparsity and total variation," *IEEE J. Sel. Topics Appl. Earth Observ. Remote Sens.*, vol. 9, no. 9, pp. 4257–4266, Sep. 2016.
- [54] J.-J. Wang, T.-Z. Huang, J. Huang, H.-X. Dou, L.-J. Deng, and X.-L. Zhao, "Row-sparsity spectral unmixing via total variation," *IEEE J. Sel. Topics Appl. Earth Observ. Remote Sens.*, vol. 12, no. 12, pp. 5009–5022, Dec. 2019.
- [55] Y. Yuan, Z. Zhang, and Q. Wang, "Improved collaborative non-negative matrix factorization and total variation for hyperspectral unmixing," *IEEE J. Sel. Topics Appl. Earth Observ. Remote Sens.*, vol. 13, pp. 998–1010, Mar. 2020.
- [56] A. Sandryhaila and J. M. F. Moura, "Discrete signal processing on graphs," *IEEE Trans. Signal Process.*, vol. 61, no. 7, pp. 1644–1656, 2013.
- [57] D. I. Shuman, S. K. Narang, P. Frossard, A. Ortega, and P. Vandergheynst, "The emerging field of signal processing on graphs: Extending high-dimensional data analysis to networks and other irregular

- domains," *IEEE Signal Process. Mag.*, vol. 30, no. 3, pp. 83–98, May 2013.
- [58] A. Ortega, P. Frossard, J. Kovačević, J. M. F. Moura, and P. Vandergheynst, "Graph signal processing: Overview, challenges, and applications," *Proc. the IEEE*, vol. 106, no. 5, pp. 808–828, 2018.
- [59] Y. Tanaka, Y. C. Eldar, A. Ortega, and G. Cheung, "Sampling signals on graphs: From theory to applications," *IEEE Signal Process. Mag.*, vol. 37, no. 6, pp. 14–30, 2020.
- [60] G. Gilboa and S. Osher, "Nonlocal operators with applications to image processing," *Multiscale Model. Simul.*, vol. 7, no. 3, pp. 1005–1028, 2009.
- [61] S. Ono, I. Yamada, and I. Kumazawa, "Total generalized variation for graph signals," in *Proc. IEEE Int. Conf. Acoust., Speech Signal Process. (ICASSP)*, 2015, pp. 5456–5460.
- [62] P. Berger, G. Hannak, and G. Matz, "Graph signal recovery via primal-dual algorithms for total variation minimization," *IEEE J. Sel. Topics Signal Process.*, vol. 11, no. 6, pp. 842–855, Sep. 2017.
- [63] Z. Li, F. Malgouyres, and T. Zeng, "Regularized non-local total variation and application in image restoration," *J. Math. Imag. Vis.*, vol. 59, no. 2, pp. 296–317, 2017.
- [64] B. Li, Y.-K. Lai, and P. L. Rosin, "Sparse graph regularized mesh color edit propagation," *IEEE Trans. Image Process.*, vol. 29, pp. 5408–5419, 2020.
- [65] N. Perraudin, J. Paratte, D. Shuman, L. Martin, V. Kalofolias, P. Vandergheynst, and D. K. Hammond, "GSPBOX: A toolbox for signal processing on graphs," *ArXiv e-prints*, 2014.



Kazuki Naganuma Kazuki Naganuma (S'21) received a B.E. degree and M.E. degree in Information and Computer Sciences in 2020 from the Kanagawa Institute of Technology and from the Tokyo Institute of Technology, respectively.

He is currently pursuing a Ph.D. degree at the Department of Computer Science in the Tokyo Institute of Technology. His current research interests are in signal and image processing and optimization theory.



Shunsuke Ono (S'11–M'15) received a B.E. degree in Computer Science in 2010 and M.E. and Ph.D. degrees in Communications and Computer Engineering in 2012 and 2014 from the Tokyo Institute of Technology, respectively.

From April 2012 to September 2014, he was a Research Fellow (DC1) of the Japan Society for the Promotion of Science (JSPS). He is currently an Associate Professor in the Department of Computer Science, School of Computing, Tokyo Institute of Technology. From October 2016 to March 2020 and from October 2021 to present, he was/is a Researcher of Precursory Research for Embryonic Science and Technology (PRESTO), Japan Science and Technology Corporation (JST), Tokyo, Japan. His research interests include signal processing, image analysis, remote sensing, mathematical optimization, and data science.

Dr. Ono received the Young Researchers' Award and the Excellent Paper Award from the IEICE in 2013 and 2014, respectively, the Outstanding Student Journal Paper Award and the Young Author Best Paper Award from the IEEE SPS Japan Chapter in 2014 and 2020, respectively, the Funai Research Award from the Funai Foundation in 2017, the Ando Incentive Prize from the Foundation of Ando Laboratory in 2021, and the Young Scientists' Award from MEXT in 2022. He has been an Associate Editor of IEEE TRANSACTIONS ON SIGNAL AND INFORMATION PROCESSING OVER NETWORKS since 2019.